University of Turku/ Åbo Akademi

Faculty of Medicine

Imaging of *Salmonella* infection at a single cell resolution

Submitted By: Alaa Benkherouf

Student number: 523389

Email: albenk@utu.fi

Site of research: Faculty of Medicine, Medisiina D7

Responsible professor: Riku Klén, PhD, Assistant Professor

Supervised By:

Arto Pulliainen, PhD, Docent (Molecular Microbiology), Institute of Biomedicine, Infection and Immunity Unit, head of Turku Cellular Microbiology Laboratory (TCML)

July 2022

Abstract

Salmonella is a rod-shaped bacterium that infects many cells including macrophages in the gastrointestinal tract and causes salmonellosis. Single-cell technologies are being utilised to study the heterogeneity of host-pathogen interactions, which focus on unravelling the different experiences *Salmonella* goes through during infection within the same host. ADP-ribosylation is the process of transferring of ADP-ribose from NAD^+ onto a target molecule and is catalysed by PARPs. PARPs have many roles including inflammation and host–pathogen interactions, yet it is hardly studied when comes to bacterial infections. It is involved in M1/M2 polarisation of macrophages, but on the other hand, *Salmonella* is known to favour M2 polarised macrophages for long term persistence. In an ongoing study in the host laboratory (TCML), PARP14 was found to be upregulated in *Salmonella* infected macrophages in vitro. The aim of this study is to optimise *in vitro* conditions to monitor *Salmonella*-macrophage interaction at a single cell resolution and the possible heterogeneity within. Subsequent aim is to determine the functional importance of ADP-ribosylation-mediated cell signalling processes to *Salmonella*-macrophage interaction using pharmaceutical inhibition of PARP-enzymes. Flow cytometry was employed to optimise the MOI of *Salmonella* SL1344-GFP and PARP inhibitor PJ34 concentration. For single-cell visualisation, epifluorescence microscopy was used. Automated batch image analysis was done using ImageJ macro that calculated the number of bacteria and cells per coverslip. A manual approach was implemented to calculate the number of bacteria per cell. After optimising the experiment conditions, the chosen MOI was 100 to be able to visualise Salmonella-macrophage interaction. For the functional importance of PARPs, a concentration of 50 μM was chosen for PJ34 because higher concentrations were causing interference in flowcytometry with the SL-1344-GFP signal. Results from flowcytometry revealed that during salmonellosis, PJ34 treatment showed more cells associated with bacteria than non-treated cells at 6 hours, yet this difference was not significant indication that PJ34 has no major effects on salmonellosis. Epifluorescence microscopy showed the heterogenous nature of infection that is characterised by the different number of bacteria per infected cell.

Keywords: Salmonella, ADP-ribosylation, PJ34, PARPs, salmonellosis, imaging

List of Abbreviations

Minimum inhibitory concentration (MIC)

Interleukin-10 (IL-10).

Interferon-γ (IFN-γ)

Salmonella pathogenicity island 2 (SPI-2)

Type III secretion system (T3SS)

Non-typhoidal serotypes (NTS).

Salmonella enterica serovars Typhi (S. Typhi),

Salmonella Paratyphi (S. paratyphi),

Salmonella Sendai (S. Sendai)

Invasive non-typhoidal *Salmonella* (iNTS)

Serovar Typhimurium (S. Typhimurium)

Salmonella Pathogenicity Island-1 (SPI-1)

Type III Secretion system (T3SS)

Microfold (M) cells

Salmonella Pathogenicity Island-2 (SPI-II)

Mesenteric lymph node (MLN)

Salmonella-containing vacuole (SCV)

Endosomal antigen 1 (EEA1)

Lysosomal glycoprotein 1 (LAMP-1)

Salmonella inducing filaments (Sifs)

Classically activated macrophages (CAM)

Alternatively activated macrophages (AAM)

Lipopolysaccharide (LPS)

Interferon gamma γ (IFNγ)

Interleukin 4 (IL-4)

ADP-ribosylation (ADPr)

post-translational modification (PTM)

ADP-ribose transferases (ARTs)

Poly-ADP-ribose polymerases (PARPs)

ADP-ribosyltransferases diphtheria toxin-like (ARTDs)

Nicotinamide adenine dinucleotide (NAD^+)

Poly-ADP-ribosylation (PARylation)

Mono-ADP-ribosylation (MARylation)

ADP-ribosyl transferases (ARTCs)

ADP-ribosyl transferases (ARTDs)

H-Y-E (histidine, tyrosine, glutamate)

R-S-E (arginine, serine, glutamate)

Signal Transducer and Activator of Transcription 6 (STAT6)

PARP inhibitor VIII or PJ-34 ([N-(6-oxo-5,6-dihydrophenanthridin-2-yl)-N,N-dimethylacetamide.HCl])

Interleukin-6 (IL-6)

Light microscopy techniques (LM)

Wide field microscopy (WFM)

Live cell imaging (LCI)

Confocal laser scanning microscopy (CLSM)

Spinning disk confocal microscopy (SDCM)

Photomultiplier tube (PMT)

Fluorescence recovery after photobleaching (FRAP)

Electron microscopy (EM)

Transmission electron microscopy (TEM)

Scanning electron microscopy (SEM)

Multiphoton microscopy (MP)

Surface plasmon resonance imaging (SPRi)

Multiplicity of infection (MOI)

Abelson Murine Leukemia Virus (A-MuLV)

Dulbecco's modified eagle medium (DMEM)

Fetal bovine serum (FBS)

Dimethyl sulfoxide (DMSO)

PBS (Phosphate buffered saline 1x 0.00067M (PO_4))

Luria Bertani (LB)

Optic density (OD)

Forward scatter (FSC)

Side scatter (SSC)

Praformaldehyde (PFA)

4′,6-diamidino-2-phenylindole (DAPI)

Red-green-blue (RGB)

Uninfected (UI)

Infected (I)

Green fluorescent protein (GFP)

List of figures

Table of Contents

1. Literature review

1.1 Bacterial persistence

Antibiotic resistance has been and will continue to be one of the most important challenges facing scientists in the following decades. This might be because of genetically acquired resistance modifications, poor pharmacokinetics of antibiotics or persistence of bacteria. (Gollan et al., 2019) Many types of bacteria can inhabit their hosts and remain there for long periods of time, and this phenomenon is known as persistence. (Fisher et al., 2017) Another important definition in this field is bacterial persisters, which is an antibiotic-tolerant subset of bacteria that is slow-growing or growth-arrested and is less susceptible to killing by bactericidal antibiotics within susceptible populations as a result of low target activity or low antibiotic uptake induced by stress. (Fisher et al., 2017) It also involves the ability of bacteria to survive intracellularly during host immune responses and drugs, including antibiotics; those are known as antibiotic persisters. They can persist through growth-affecting arrest, and because of their non-growing heterogenous phenomena, their presence does not affect the minimum inhibitory concentration (MIC) of the whole population. (Gollan et al., 2019)

There are many reasons that justify the ability of bacteria to persist within a host. One reason is the inability of failure of the host immune system to eliminate and clear out the bacteria because the latter have developed strategies that enables them to passively avoid being detected by the host. For example, *Borrelia spp.* can vary surface antigens during infection. (Fisher et al., 2017) Some bacteria also have the ability to modulate or manipulate host immune responses by triggering inapt pathways in the anti-inflammatory immune response, which decreases the chances of pathogen clearance. (Fisher et al., 2017) Examples of such pathogens include *Listeria monocytogenes* and *Mycobacterium tuberculosis*, which can trigger an anti-inflammatory immune response by inducing the production of interleukin-10 (IL-10). This will lead to the suppression the interferon-γ (IFN-γ) production in macrophages, which generally functions on inhibiting bacterial growth. (Huemer et al., 2020) Pathogens including *M.tuberculosis*, *Legionella pneumophila*, and *Salmonella spp.* inhibit the maturation of phagosomes in order to avoid degradation by host immune cells. (Fisher et al., 2017) *Salmonella* is also able to interfere with adaptive immune response by *Salmonella* pathogenicity island 2 (SPI-2) type III secretion system (T3SS), which inhibits MHC class II antigen presentation in dendritic cells, which might affect T-cells in favour of the bacteria. (Scott et al., 2003; Fisher et al., 2017) Another reason for persistence is ineffective clearance by antibiotics, which could

have resulted from poor patient compliance, poor pharmacokinetics of the antibiotic, and resistance acquired through horizontal gene transfer or genetic adaptation. This enables the bacteria to survive in the host even at toxic concentrations of the antibiotic. (Fisher et al., 2017) The ability of bacteria to live in such conditions is called antibiotic tolerance.

Since tolerance, persistence and resistance have been interchangeably used in literature, it has been proposed to give each term a distinctive definition that explains the mechanism of action for each and distinguishes between them. (Brauner et al., 2016) Many scientists have defined tolerance as the decreased susceptibility of a certain bacterial population to bactericidal antibiotics that has resulted from low target or low drug uptake, which are often linked to slow growing of the bacteria or reduced metabolism that was induced by the stressful conditions. (Fisher et al., 2017; Gollan et al., 2019) It has also been defined as an increase in the amount of time it takes for an entire bacterial population to be killed by a particular antibiotic concentration. (Brauner et al., 2016) Antibiotic resistance is defined as the ability of a bacterial population to proliferate in the presence of antibiotics due to an acquired genetic mutation that allows the antibiotic to be degraded or exported or enables the modification of the antibiotic target. (Fisher et al., 2017) In other words, the bacteria can decrease the effectiveness of the antibiotic, so by increasing the concentration of the antibiotic, the same effect on susceptible strains might be seen on resistant strains. (Brauner et al., 2016) Resistance to antibiotics can be found either within a population or within a subpopulation by phenotypic heterogeneity. (Fisher et al., 2017) Recent single-cell technologies have been used to further study the heterogeneity of infections and reveal the host-pathogen diversity within the host tissue. (Bumann and Cunrath., 2017) One example of infection heterogeneity and persistence is *Salmonella* Typhimurium, in which it is believed that *Salmonella* infects the host cells differently and remain dormant or growth-arrested until they can re-establish growth when cellular stress pathways are deactivated. (Bumann and Cunrath., 2017; Fisher et al., 2017) Since *Salmonella* heterogeneity is a newly emerging field, many models including animal and cell culture models along with molecular biology will be able to give further insight into the divergent outcomes of individual encounters. (Bumann and Cunrath., 2017)

1.2 *Salmonella* bacterium and pathogenesis

Salmonella is a Gram-negative facultative anaerobe that can infect a variety of animals, including humans, through contaminated food. (Wang et al., 2020) With approximately 2600 serovars identified to date, *Salmonella enterica* (S. enterica) is the most pathogenic species. (Jajere, 2019) When it comes to human infections, *Salmonella* is divided into two groups: typhoidal serotypes and thousands of non-typhoidal serotypes (NTS). Typhoid disease is caused by *Salmonella enterica* serovars Typhi (S. Typhi), Paratyphi (S. paratyphi), and Sendai (S. Sendai), with serovars Typhimurium (S. Typhimurium) being one of the most common NTS. (Balasubramanian et al., 2019; Wang et al., 2020) The most common symptoms of NTS infection are gastroenteritis, diarrhea, and fever, with a low fatality rate. (Deborah A. Adams1; Kimberly R. Thomas, 2015; Wang et al., 2020) Non-typhoidal *Salmonella* infections can penetrate typically sterile parts of the body, causing bacteraemia, meningitis, and other localized infections in addition to diarrhea. (Wang et al., 2020) Invasive non-typhoidal *Salmonella* (iNTS) infection is characterised by a nonspecific fever that is comparable to malaria and other febrile illnesses, resulting in being clinically indistinguishable infections with a higher fatality rate than non-invasive infections. (Stanaway et al., 2019; Crump et al., 2015)

Distinct *Salmonella* serotypes have different hosts, dietary sources, and pathophysiology, making control difficult and complicated. (Wang et al., 2020) In this model, the *Salmonella enterica serovar* Typhimurium (S. Typhimurium), which is an intracellular bacterium that colonises varies types of cells including epithelial cells, fibroblasts, macrophages, and dendritic cells. (Knodler, 2015) After the ingestion of contaminated food or water, the journey of *Salmonella* begins. As soon as it reaches the stomach, it increases its intracellular pH to tolerate the acidity in the stomach. (dos Santos et al., 2019) It then crosses the mucus layer in the intestinal wall, and that is when the clinical features are apparent. *Salmonella* then adheres to the host cell by host-receptor interactions with many adhesion factors present on the cell surface of this bacterium. By the action of proteins encoded by *Salmonella* Pathogenicity Island-1 (SPI-1), *Salmonella* releases effector proteins through a molecular apparatus called the Type III Secretion system (T3SS). (dos Santos et al., 2019) T3SS-1 forms a translocation pore in the host cell membrane, using a needle structure, and transports the effector proteins that are responsible for actin rearrangement. (dos Santos et al., 2019) Another way of entry of *Salmonella* into host cells is transcytosis through the Microfold (M) cells of Peyer's patch in the small intestine, which passively takes up the bacteria from the lumen to the

basolateral side by the M cells. (Pradhan and Devi Negi, 2019) About 10% of the cells in Peyer's patch are M cells that have the inner side facing the lumen and the outer side containing lymphocytes and phagocytes. (Pradhan and Devi Negi, 2019) This is followed by inflammation, which causes immune cells such neutrophils, T and B cells, dendritic cells, and macrophages to infiltrate the entry site. T3SS-II effector proteins encoded by *Salmonella* Pathogenicity Island-2 (SPI-II) help in the survival of the internalised bacteria in these cells. By crossing the epithelial barrier, these bacteria move from M cells to enterocytes. They are subsequently phagocytised by immune cells in the lamina propria and migrate through the blood and lymphatic system to the mesenteric lymph node (MLN), from where they travel to deeper tissues such the spleen, liver, and bone marrow. In all these tissues, bacteria reside inside the macrophages in compartments called *Salmonella*-containing vacuole (SCV), where they can survive and multiply since those vacuoles are protected from the host antimicrobial defence mechanisms. (Gog et al., 2012; dos Santos et al., 2019; Pradhan and Devi Negi, 2019) Early SCV expresses endosomal markers such as endosomal antigen 1 (EEA1) in the early stages of maturation, however these early protein markers are quickly replaced by late endosomal markers such as lysosomal glycoprotein 1 (LAMP-1). (Gog et al., 2012) If several bacteria infect a cell at the same time, they will be housed in the same SCV. If two separate infections occurred at different periods, one may anticipate the bacteria to be housed in various SCVs, exhibiting endosomal markers indicating different stages of maturity within the same cell. This process is briefly explained in figure 1.

Salmonella establishes a network of interconnected tubules termed *Salmonella* inducing filaments (Sifs) to gain access to membrane components and nutrients from the host endocytic compartments. (Sindhwani et al., 2017) *Salmonella* avoids SCV-lysosome fusion, resulting in a better environment for survival and proliferation. Finally, macrophage apoptosis releases the *Salmonella* which then re-infects nearby epithelial cells or other phagocytic cells of the host immune system. *Salmonella* has the ability to persist in MLN, spleen, and liver for years from where the infection took place. (Pradhan and Devi Negi, 2019)

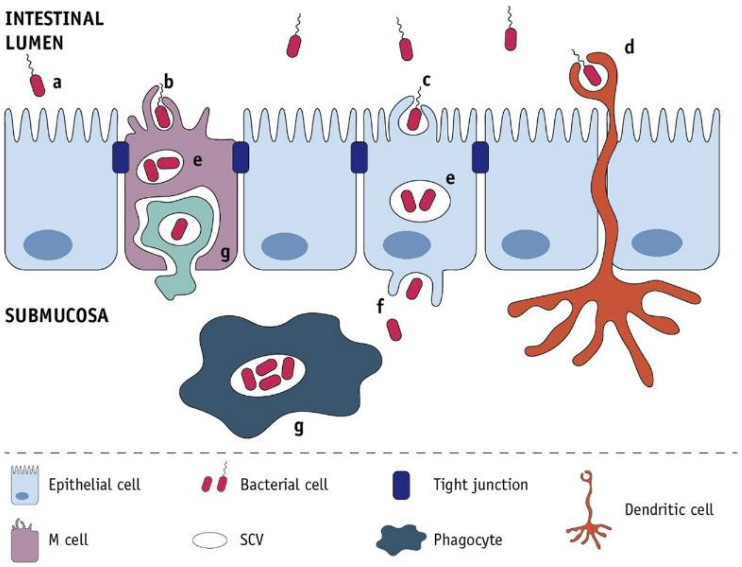

Figure 1: *Salmonella* pathogenesis: *Salmonella* adheres to the intestinal epithelium using adhesion factors on its surface to change the cytoskeleton of the enterocytes and lead to the formation of ruffles. This process enables dendritic cells to take the bacteria directly from the submucosa. At this stage, the bacteria are located in *Salmonella* containing vacuoles (SCV) in which they multiply. The SCV transcytose and are released into the submucosa where they are phagocytised by phagocytes. (dos Santos et al., 2019)

1.3 Macrophage selection

Macrophages are immune cells that help maintain homeostasis and combat pathogen invasion. Macrophages in various tissues become polarised when their environment changes, resulting in diverse macrophage subtypes. (Yunna et al., 2020) Macrophages are also responsible for the removal of cellular debris formed during tissue remodelling, as well as the rapid and effective clearance of apoptotic cells by phagocytosis. (Mosser and Edwards, 2008)

Based on their function, macrophages were classified into M1 or classically activated macrophages (CAM), and M2 or alternatively activated macrophages (AAM). (Gogoi et al., 2019; Yunna et al., 2020) Lipopolysaccharide (LPS), which is present in microbes, and cytokines such as interferon gamma γ (IFNγ) have the ability to drive macrophage polarisation to the M1 phenotype leading to the secretion of pro-inflammatory cytokines to assist the host in fighting the infection, while interleukin-4 (IL-4) can induce macrophage polarisation to M2 resulting in the secretion of anti-inflammatory cytokines, which are essential for resolving inflammation and wound

healing. (Murray et al., 2014; Gogoi et al., 2019) Many pathogens have taken the lack of microbial activity in M2 as an advantage to persist and proliferate inside the host. (Brodsky, 2020) Studies have shown that *Salmonella* prefers inhabiting the M2 macrophages or AAM during the establishment of chronic infections. (Gogoi et al., 2019) *Salmonella* among other pathogens possess effector proteins that take over the M1 polarising stimuli that takes place during infection and induce infected macrophages in culture to switch to an M2-like polarisation state. (Brodsky, 2020) After the inspection of infected macrophages using dual RNA-seq data, the up-regulation of M1 activation markers were dampened, but M2 activation markers were highly expressed in macrophages containing viable bacteria. (Fisher et al., 2018)

1.4 ADP-ribosylation and PARPs

ADP-ribosylation (ADPr) is a reversible chemical post-translational modification (PTM) of proteins found across all domains of life including viruses, bacteria, and eukaryotes, and known to regulate a variety of cellular processes, including DNA repair, cell proliferation and differentiation, metabolism, stress, immune responses, transcription, telomere dynamics and cell death. (Michael S Cohen, 2017; Crawford et al., 2018; Palazzo et al., 2019; Groslambert et al., 2021) ADPr is the enzymatic transfer of single or multiple ADP-ribose moiety by the catalytic action of ADP-ribose transferases (ARTs) or also known as poly-ADP-ribose polymerases (PARPs) and in some literature called ADP-ribosyltransferases diphtheria toxin-like (ARTDs), which are enzymes that catalyse ADPr. Those ADP-ribose moiety are transferred from nicotinamide adenine dinucleotide (NAD^+) onto a target substrate amino-acid, releasing nicotinamide in the process (Figure 2). (Michael S Cohen, 2017; Miettinen et al., 2019; Palazzo et al., 2019; Groslambert et al., 2021) This PTM can take place as mono-ADP-ribosylation (MARylation) or can be as linear or branched poly-ADP-ribosylation (PARylation). (Miettinen et al., 2019)

Returning to ADP-ribosyltransferases, they are classified into two superfamilies of enzymes: the cholera toxin-like ADP-ribosyl transferases (ARTCs) and the diphtheria toxin-like ADP-ribosyl transferases (ARTDs). The protein fold of these two types of enzymes is evolutionarily conserved, and it is known as the ART domain, which is made up of two core β-sheets, one anti-parallel sheet with three to five β strands, and one sheet with four to five β strands. (Palazzo et al., 2019) The connection between ARTCs and

ATRDs is defined by three important amino acids; the R-S-E (arginine, serine, glutamate) in bacterial RSE ARTs and H-Y-E (histidine, tyrosine, glutamate) in bacterial HYE ARTs, respectively. (Michael S Cohen, 2017; Palazzo et al., 2019) RSE ARTs are also referred to as ARTDs, and HYE ARTs are also referred to as ARTCs. In humans, two ART families are homolog to bacterial ARTs: PARPs and ectoARTs. PARPs are also considered as ARTDs since they are related to HYE ARTs. (Michael S Cohen, 2017)

At this moment, studies have shown that humans express 21 ARTs; 17 of them being PARPs (or ARTDs) and 4 being ARTC proteins (Michael S Cohen, 2017; Palazzo et al., 2019) Among the 17 human PARPs, PARP1, PARP2, PARP5A, and PARP5B catalyse PARylation, whereas the majority of the others (such as PARP14 and PARP15) catalyse MARylation. (Fehr et al., 2020) PARP1 has been the subject of practically all studies on the functional involvement of mammalian PARPs in acute and chronic bacterial infections. (Miettinen et al., 2019) In an oral *S.typhi* mouse model, research showed that the absence of PARP1 causes a delay in immune system's proinflammatory response. (Miettinen et al., 2019) A gene ontology study of the entire genome microarray data indicated that many of the PARP1-dependent genes were known immune response genes, specifically those implicated in IFN-γ signalling, which in turn indicates that PARP1 may be involved in the recruitment of immune cells during salmonellosis. (Toller et al., 2010; Kunze et al., 2019; Miettinen et al., 2019)

In vitro experiments show that PARP14, also known as ARTD8, plays a role in *Salmonella* gut infection, particularly in macrophages. (Miettinen et al., 2019) PARP14 was designated Co-activator of Signal Transducer and Activator of Transcription 6 (STAT6) after it was discovered to be an interactor and transcriptional collaborator for STAT6 (CoaSt6). (Goenka and Boothby, 2006) PARP14 is primarily involved in the transcription of interleukin-4 (IL4)-responsive genes, which regulate cell survival, metabolism, and proliferation. (Cho et al., 2009; Caprara et al., 2018) Silencing PARP14 increases proinflammatory gene expression and STAT1 phosphorylation in M(IFN-γ) cells while suppressing anti-inflammatory gene expression and STAT6 phosphorylation in M(IL-4) cells. (Iwata et al., 2016) Other *in vitro* studies have shown that PARP14 inhibits proinflammatory IFN–STAT1 signalling and stimulates the anti-inflammatory IL-4-STAT6 pathway in primary human macrophages. (Fehr et al., 2020) In comparison to parental cells, PARP14-deficient RAW264.7 macrophages had more viable intracellular *Salmonella*, implying that the presence of PARP-14 inhibits *Salmonella*

growth in macrophages. (Caprara et al., 2018) The exact importance of PARP-14 for salmonellosis is still to be uncovered in future research.

Many ADP-ribosylation studies have used PARP-1 inhibitor PJ-34 or PARP inhibitor VIII ([N-(6-oxo-5,6-dihydrophenanthridin-2-yl)-N,N-dimethylacetamide.HCl]) in order to understand the functional importance of PARP-1/2 for numerous inflammatory diseases including cancer, cardiovascular disorders, and neuropathies. (Henning et al., 2018; Xu et al., 2019; Mekhaeil et al., 2022) A study was conducted in 2009 using PJ-34 to study salmonellosis and the upregulation of interleukin-6 (IL-6) by enterocytes during infection, which in turn opened the door for PJ-34 to be experimented with in regards of human inflammatory diseases. (Huang, 2009) PARP knockdowns and knockouts have also been used in cancer research and infectious and inflammatory diseases research. (Li et al., 2016; Gutierrez et al., 2016; Vida et al., 2018; Peng et al., 2019)

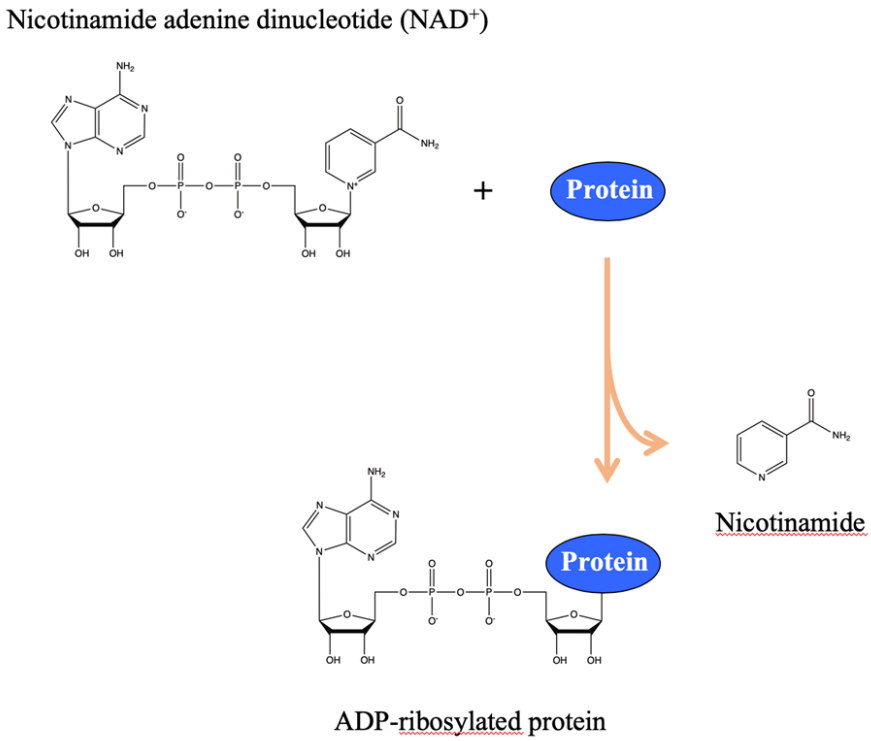

Figure 2: ADP ribosylation schematic: This figure briefly explains the ADP-ribosylation process, which includes a reaction between NAD^+ and a protein, which in turn yields an ADP-ribosylated protein with the release of nicotinamide. (Miettinen et al., 2019)

1.5 Salmonellosis imaging

In order to study *Salmonella* infection at a single cell level, researchers have used many imaging methods in models ranging from whole animal to isolated cells since those techniques uniquely allowed researchers to examine bacterial-host cell interactions at the single-cell and single-event level. Light microscopy techniques (LM), such as conventional phase-contrast, fluorescence, and confocal laser scanning microscopy, are more commonly employed to examine bacteria's interactions with cells because they are more accessible, and while they lack the resolution of other techniques, they are more versatile and may be used to study dynamic processes in living cells. (Perrett and Jepson, 2007) Wide field microscopy (WFM) or conventional light microscopy in its most basic form can acquire a simple image with a system that consists of a typical upright or inverted microscope and a camera (e.g., CCD camera). (Malt et al., 2015) WFM imaging systems are highly flexible; for example, shuttering, focus drives, and filter changers may be included to allow the user to automate rapid switching between imaging parameters. Due to these qualities, as well as the high sensitivity of camera systems, which allows for rapid image acquisition and minimal light exposure making WFM the most popular choice for live cell imaging (LCI). (Malt et al., 2015) WFM is a good technique to study *Salmonella* biology aside from infection since it can be used to study bacteria within a narrow focal depth in suspension or on agar-coated coverslips. (Malt et al., 2015) WFM has also been used to study *Salmonella* SPI gene expression and how it affects growth rates. (Sturm et al., 2011) Real time imaging of live cells in culture during infection revealed that the host cells go through different encounters during infection, which enabled the visualisation of the heterogeneous subsets of the intracellular slow- and fast-growing *Salmonella*. (Pucciarelli and García-del Portillo, 2017) *Salmonella* adhesion, membrane ruffling, SCV biogenesis, and replication dynamics within infected cells have all been demonstrated using live cell and fixed cell microscopy. Microscopy advances, as well as the development of fluorescent protein-based reporters, have aided in the separation of signalling and trafficking events in infected cells. Additionally, GFP-based reporters and microscopy have helped researchers better understand virulence gene expression and heterogeneity within populations. (Malt et al., 2015)

Confocal microscopy has been a routine research technique since its launch in the 1980s, with CLSM systems in particular being widely available. (Malt et al., 2015) Confocal microscopy systems are classified into two types: confocal laser scanning microscopy (CLSM) and spinning disk confocal microscopy (SDCM). (Kehl and Hensel,

2015) In CLSM, as a laser scans across a field of vision, an image of fluorescence is acquired point-by-point, or less commonly line-by-line. Light emitted by the sample travels in the opposite direction, passing through an aperture or a single pinhole on its way to a detector, often a photomultiplier tube (PMT). (Kehl and Hensel, 2015; Malt et al., 2015) The confocal aperture allows light from only one plane of focus to reach the detector, allowing for optical sectioning, which improves axial resolution and gives CLSM a significant advantage over WFM. (Malt et al., 2015) Most CLSMs can detect multiple fluorophores at the same time by the selective direction of different wavelengths of emitted light to different detectors. (Malt et al., 2015) CLSM can also control the scan geometry in techniques that require selective illumination of specific areas in a section. An example of selective illumination is selective photobleaching, which can be used in mobility testing of GFP-labelled proteins using fluorescence recovery after photobleaching (FRAP). (Malt et al., 2015) On the other hand, SDCM uses a rotating Nipkow disk with multiple pinholes, which uses a camera to detect emitted light from the whole field while limiting detection to a single level of focus. (Kehl and Hensel, 2015; Malt et al., 2015) Although SDCM are faster and at low risk of causing photo damage to samples, they are less adaptable in terms of magnification and depth of focus and have less axial resolution than CLSM. (Malt et al., 2015) CLSM has been used to identify *Salmonella* attached to and within M cells in intact Peyer's patch tissue preparations. (van Engelenburg and Palmer, 2010) It has also been used to study vacuolar and cytosolic *Salmonella* and the presence of cytosolic *Salmonella*-infected cells within the lumen of the gastrointestinal tract of mice. (Knodler et al., 2014a; Knodler, 2015) Spinning disk systems are an excellent alternative to WFM for imaging with better axial resolution, and they have been utilised extensively for live cell imaging of salmonellosis in cultured cells as well as imaging *Salmonella* biofilms. (Knodler et al., 2010; Grantcharova et al., 2010; Malik-Kale et al., 2012) Confocal microscopy has also been used to study the heterogeneity of *Salmonella*-host interaction in infected host tissue. (Bumann and Cunrath, 2017)

Another important imaging technique for *Salmonella* research is electron microscopy (EM), which is a nanomaterial characterisation tool that can provide valuable insights into biological systems, such as cells labelled proteins in cells, as well as materials science processes, such as nanoparticle creation and electrochemical deposition. (de Jonge and Ross, 2011; Malt et al., 2015; Picó, 2018) When the sample interacts with an electron beam, an electron micrograph is created, which can then be processed into

images. Electron energy, material density, atomic number of elements, and the material's surface topography are all factors that influence this interaction. (de Jonge and Ross, 2011)The exact location of *Salmonella* and its interaction to cellular components can be revealed using electron microscopy and confocal microscopy. (Malt et al., 2015) Transmission electron microscopy (TEM) offers morphological information on *Salmonella* surface structures such as pili, flagella and T3SS, and when combined with advanced image analysis and processing, it yields high resolution molecular level structural information. (Bergeron et al., 2013; Malt et al., 2015) It has also been used to study the compartmentalisation of *Salmonella*, and when combining TEM with light microscopy, it can be used for the ultrastructural examination of labelled features during infection, which in turn would provide extensive information on what happens during vacuole lysis inside cells. (Kageyama et al., 2011; Knodler et al., 2014b; Mellouk et al., 2014; Knodler, 2015) Scanning electron microscopy (SEM) produces detailed high-resolution images of the specimen by concentrating an electron beam across the surface and collecting secondary or backscattered electron signals. SEM offers ultrastructure of the apical side of *Salmonella*-infected host cells with the best resolution of surface features of the infected cells. (Carina Kommnick, 2021) It has also been used to search for cell surface or bacterial shape alterations to study immunogenic potential of bacterial flagella for *Salmonella*-mediated tumour therapy. (Felgner et al., 2020)

Other imaging techniques that were used to study *Salmonella* infection are multiphoton microscopy (MP), surface plasmon resonance imaging (SPRi), flowcytometry and epifluorescence microscopy. MP microscopy has higher penetration of longer wavelength light enabling it to be used to examine fluorescent substances deep within complex environments, and thus has potential applications in investigating the dynamics of host-pathogen interactions during infection of intact tissues, as well as intricate biofilm structure. It has been used to study the recruitment of dendritic cells into the intestinal epithelium of living mice during salmonellosis. (Malt et al., 2015) SPR is a label-free optical technology based on the surface plasmon resonance phenomenon that occurs at the interface of thin metallic films and a dielectric such as buffers. It can detect a wide range of interactions, such as nucleic acid hybridisation, antibody-epitope binding, protein-carbohydrate, protein-protein, and protein-DNA interactions. Its uses in clinical diagnostics, environmental monitoring, and food safety detection have all been reported. In *Salmonella* research, it has been used to build an assay that can detect foodborne *Salmonella* with minimal specimen preparation and without screening labels.

(Chen and Park, 2018) Cell culture, flowcytometry, epifluorescence microscopy and image analysis combined can be used to study salmonellosis at a single cell level. (Helaine et al., 2010; Fernandes et al., 2014; Malt et al., 2015; Antoniou et al., 2019)

2. Aims and objectives

Salmonella can breach the host barriers and manipulate the host immune response enabling it to persist within the host cells and withstand stressful environmental conditions. Until recently, researchers have started paying more attention on host-*Salmonella* interaction and how this pathogen changes its metabolism inside the host in a way that affects the course of infection and allows it to combat the host immune response. After days of infection, *Salmonella* can be found within colonic epithelial cells and within macrophages, which raises the main question as to why the macrophages are not killing the bacterium as it should be in the first place.

The first aim of this study is to optimise *in vitro* conditions to monitor *Salmonella*-macrophage interaction at single cell resolution and the possible heterogeneity within.

Eukaryotic cells express intracellular and extracellular ADP-ribosyltransferases or poly-ADP-ribosylpolytransferases (PARPs) that catalyse ADP-ribosylation. Even though 18 PARPs have been discovered until now, yet almost only PARP1 and PARP2 have been studied in regards of DNA damage. Evidence indicates that PARPs also regulate the sterile and infectious inflammatory response, even under no apparent DNA damage. In ongoing research in the host laboratory, they screened for all PARPs during salmonellosis, and found that PARP14 was upregulated.

The second aim of this research is to determine the functional importance of ADP-ribosylation-mediated cell signalling processes to *Salmonella*-macrophage interaction using pharmaceutical inhibition of PARP-enzymes.

3. Materials and methods

3.1 Cell culture

RAW264.7 cells were used, which are mouse monocyte macrophages that were established from a tumour induced by the Abelson Murine Leukemia Virus (A-MuLV). Applications of this cell line include metabolic studies, high efficiency for DNA transfection and sensitivity to RNA interference. It has also been used for internalisation and survival of many types of bacteria. (Sigma-Aldrich, 2021) The cells were grown in Dulbecco's modified eagle medium (DMEM, Lonza, BioWhitter) enriched with 25mM HEPES, 4,5 g/L glucose, 1x L-glutamine (100x Glutamax, Gibco) and 10% fetal bovine serum (FBS), and 100 U/ml from Pen/Strep.

RAW264.7 in 10% dimethyl sulfoxide (DMSO) with a passage 3 were retrieved on ice from liquid nitrogen storage tank (-196 degrees Celsius). The tube was thawed at 37 degrees and suspended into a centrifuge tube containing 10 ml of pre-warmed DMEM. It was then centrifuged at 200 g for 20 minutes at 20 degrees. After that, the supernatant was removed without disturbing the pellet and then resuspended with 3 ml of fresh DMEM. 2ml from the suspension was suspended into a T75 flask containing 12 ml of the media and then brought to the incubator to grow at 37 degrees, 90% humidity and 5% carbon dioxide.

When confluency (80-90%) was reached after 3-4 days, the cells were divided to grow in two T75 flasks. First, the old culture medium was removed, and the cells were washed with PBS (Phosphate buffered saline 1x 0.00067M (PO_4)) with calcium and magnesium, Cytiva Hyclone), then proteins were broken down to detach cells using trypsin (1x Trypsin-EDTA solution, MP Biomedicals) for 3 minutes at 37 degrees and then trypsin was deactivated by 8-10 DMEM. After that, the cells were detached from the flask surface using cell scrapers because RAW264.7 cells are semi-adherent cells and do not detach from surfaces easily. The cell suspension was pipetted well inside the flask to ensure the presence of single cells and then suspended into a separate tube.

From the cell suspension, 10 µl was pipetted into an Eppendorf tube along with 10 µl of trypan blue (Trypan blue 0.4%, Biorad). From the cell-trypan blue mix, 10 µl was pipetted into each chamber of the counting slides (Counting slides, dual chamber for cell counter, Biorad) to measure the viability and number of cells per ml using an automated cell counter (TC20 Automated cell counter, Biorad). The desired cell viability was over 90%. For further experiments, $1*10^5$ cells/ml were selected with 3 ml of cell-containing media into 6-well plates ($3*10^5$ cells/well), which were incubated at 37 degrees, 90% humidity and 5% carbon dioxide overnight.

For ADP-ribosylation experiments, the cells were treated with PJ34 for 2 hours prior to infection and the media used for the rest of the experiment contained PJ34.

3.2 Bacterial growth

Salmonella enterica serovar Typhimurium SL1344 transformed with a GFP plasmid was grown in Luria Bertani (LB) broth. The antibiotic used in the broth was 50 mg/ml kanamycin to only allow the growth of kanamycin-resistant *Salmonella*. The bacteria were left to grow at 37 degrees, 250 rpm in a shaker incubator (Innova 40) in BSL-2 laboratory overnight. The following date, *Salmonella* was re-inoculated to fresh LB (1:10-1:100) containing 50 mg/ml kanamycin and left to grow in 37 degrees, 250 rpm until optic density (OD) at 600 nm reaches 0.6-0.8 (early to late logarithmic phase, invasive phase). For 1:10 dilution, it takes around 2 hours for the bacteria to reach the desired OD, and the higher we go, the longer it takes; for example, for 1:100, it takes up to 5 hours to reach the desired OD, either way, the needed OD in this case is 0.6-0.8.

3.3 Infection

Once the bacterial suspension was measured with a spectrophotometer (UV-1280, UV-VIS Spectrophotometer, ORDIOR) and 0.6-0.8 OD600 has been reached, the tube containing *Salmonella* was centrifuged at 3500 rpm, 4 degrees for 15 minutes (Heraeus Megafuge 16R Centrifuge, Thermo Scientific). Following that, the supernatant was removed, and the bacteria was washed with 1x PBS twice and resuspended with PBS and the OD is measured again. At this point, multiplicity of infection (MOI) should be calculated according to how many bacteria per cell is needed for infection of $3*10^5$ cells/well.

$$\text{Volume of bacterial suspension per well} = \frac{Desired\ MOI\ value \times number\ of\ cells\ per\ well}{Optic\ density\ (OD) \times 10^6}$$

After the acquisition of the volume, the bacterial suspension was pipetted gently through the wells, which at this point contain fresh DMEM that does not contain any antibiotics. The plates were moved gently in 8 shape 10 times, they were then spun down at 200 g for 5 minutes (Allegra X-12R Centrifuge, Beckman Coulter), and then moved to the incubator. The timepoints chosen for infection were 30 minutes, 1 hour, 6 hours and 24 hours. 30 minutes post infection, the first group of infected cells was washed with PBS, trypsinised and transferred into flowcytometry tubes, and the remaining timepoints were washed and fresh media containing 50 µg/ml gentamicin was added to them to eliminate any extracellular bacteria.

3.4 PJ34 treatment

PJ34 PARP inhibitor was primarily tested without infection due to the presence of aromatic rings in its chemical composition, which could cause autofluorescence problems or toxicity in some cases. Concentrations ranging from 10 µM to 100 µM were used. The cells were treated for 2-4 hours with DMEM containing the desired concentrations of PJ34. The cells were then washed, trypsinised and scrapped, after which they were pipetted into a flowcytometry tube. For flowcytometry, all lasers were tested but the one in question for this experiment was GFP, since the bacteria used has a GFP plasmid, and it is not appropriate to have background signal from the PARP inhibitor.

3.5 Flow cytometry

After each time point, the cells were analysed with a flow cytometer (Novocyte ACEA Biosciences). The flow cytometry analysis consisted of drawing a region around a population of cells manually or by selecting a certain shape and then applying that region to other parameters within the experiment. This was done by generating 3 main graphs in the flow cytometer in which the first one distinguishes between the good and bad looking populations and the second one separates the single cells and duplicates. It is then followed by a graph that whether the cells have GFP signal in them or not, and from the 3 graphs, only the first and third graphs were used for data analysis. At the top left of figure 3,A , the graph has the forward scatter (FSC) in the x-axis and the side scatter (SSC) in the y-axis with a gating around the most condensed part of the graph, which contains the good-looking population. It was then followed by the top right in figure 3, A

graph containing FSC in the x-axis and GFP in the y-axis, where the gating was set based on uninfected cells that do not emit any GFP signal to know when to start measuring the GFP signal for infected cells since SL1344 contains a GFP plasmid that will differentiate between infected cells and uninfected cells (Figure 3 a & b). The parameters used were 50,000 events inside the gating set on the first graph. The flowrate used was medium to fast based on how many events recorded per second. This was done for each timepoint for both infected and uninfected tubes. No fixation was done to avoid loss of cells or bacteria.

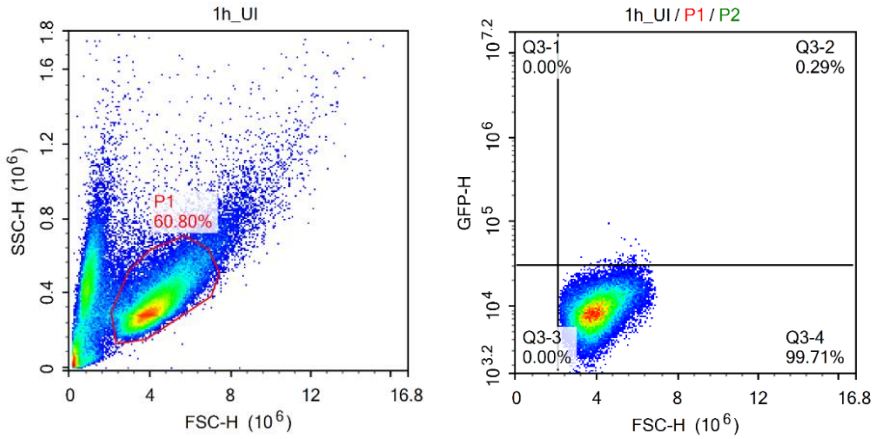

Figure 3: A. Uninfected. The graph on the left represents FSC/SSC and the graph on the right represents FSC/GFP.

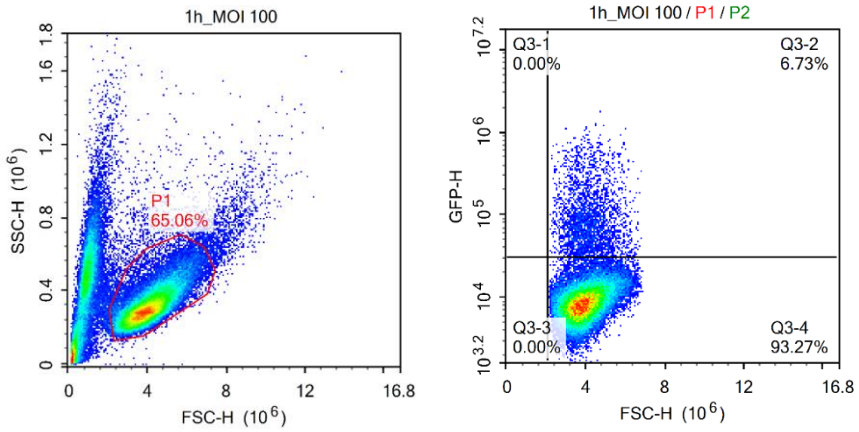

Figure 3: B. Infected. The graph on the left represents FSC/SSC and the graph on the right represents FSC/GFP.

3.6 Epifluorescence microscopy

RAW264.7 cells were seeded in 24 well plates on circular cover slips and moved to the incubator overnight at 37 degrees, 90% humidity and 5% carbon dioxide. Each timepoint, the coverslips were washed, and fixed with 5% paraformaldehyde (PFA) for 15 minutes. After that, the cells are permeabilised by 0.1% Triton for 10 minutes. This was then followed by 4′,6-diamidino-2-phenylindole (DAPI) staining with 300 nM DAPI for 1-5 minutes. Between each step, two PBS washes were performed. The coverslips were removed from the 24 well plate and mounted on slides using a Mowiol as a mounting agent. The coverslips were sealed with transparent nail polish to avoid drying. The slides were stored in foil at 4 degrees for further inspection under the microscope. Images were acquired at 63x magnification with GFP and DAPI lasers. In total for each field, 3 images were acquired; one for the blue channel, another for the green channel and the final image was a merged image for both blue and green channels.

3.7 Image analysis

The images were saved as TIFF files and analysed using ImageJ (FIJI v1.53c version). A batch macro was created to analyse whole files containing the images. The macro separates merged images into blue, green, and red channels since the option for splitting images works for RGB images. The blue channel was blurred with mean blurring to reduce noise and then thresholding was performed. After that, the nuclei were analysed, and a summary table was generated containing the number of cells and their sizes. The green channel was then analysed by thresholding and analysing the particles and a summary table was generated containing the number of bacteria present. A manual approach was used to analyse the number of bacteria per cell. A grading ranging from 0 bacteria per cell, then from 1-3, 4-6, 7-9, 9-12 and more than 12 bacteria per cell was used for all images. The analysis was made for 50 cells per subtype. The macro used for the automatic images analysis is attached in the appendix.

3.8 Data analysis

For triplicate experiments such as MOI100 and PJ34, data were gathered in percentages from flowcytometry graphs and organised in Excel (Microsoft® Excel® for Microsoft 365 MSO (16.0.13929.20222) 64-bit). The mean was generated, and then standard deviation was used to measure the variation of each data set. Following that, graphs were made using Excel with the average values and the standard deviation. For epifluorescence

microscopy values, a number of 50 cells were counted in every data set and based on those, a grading was made ranging from no bacteria per cell, 1 to 3 bacteria per cell, to 4 to 6 bacteria per cell. There was also a grading for 7 to 9 bacteria per cell, 9 to 12 bacteria per cell and more than 12 bacteria per cell for four different timepoints. A graph was then made for each timepoint to compare between different numbers of bacteria at each timepoint. A T-test was performed for one of the experiments to assess whether the difference detected was significant or not.

4. Results

4.1 GFP plasmid stability in *Salmonella* Typhimurium (SL1344-GFP) using flowcytometry.

Salmonella (SL1344) was previously transformed with GFP plasmid in order to differentiate between infected and uninfected RAW264.7 cells. The bacteria were grown until late lag phase until the optic density at 600 nm was 0.6-0.8. They were then washed twice with PBS and then analysed with flowcytometry. (Figure 4) The first graph (A) represents the cells of interest, or SL1344 without GFP in this case, which shows that there are 97.97% bacteria that fall within the drawn gate that represents the good-looking cells while excluding the debris. Graph (B) represents the populations within the gate set in graph (A), which shows that 0.69% *Salmonella* with no GFP are emitting GFP signal. The first two graphs (A & B) were used for control to check for the viability of *Salmonella* that was transformed with a GFP plasmid. Graph (C) represents the population in question and based on the chosen population in graph (C), graph (d) shows *Salmonella*-GFP signal, which is indicated by 99.85% of the transformed *Salmonella*.

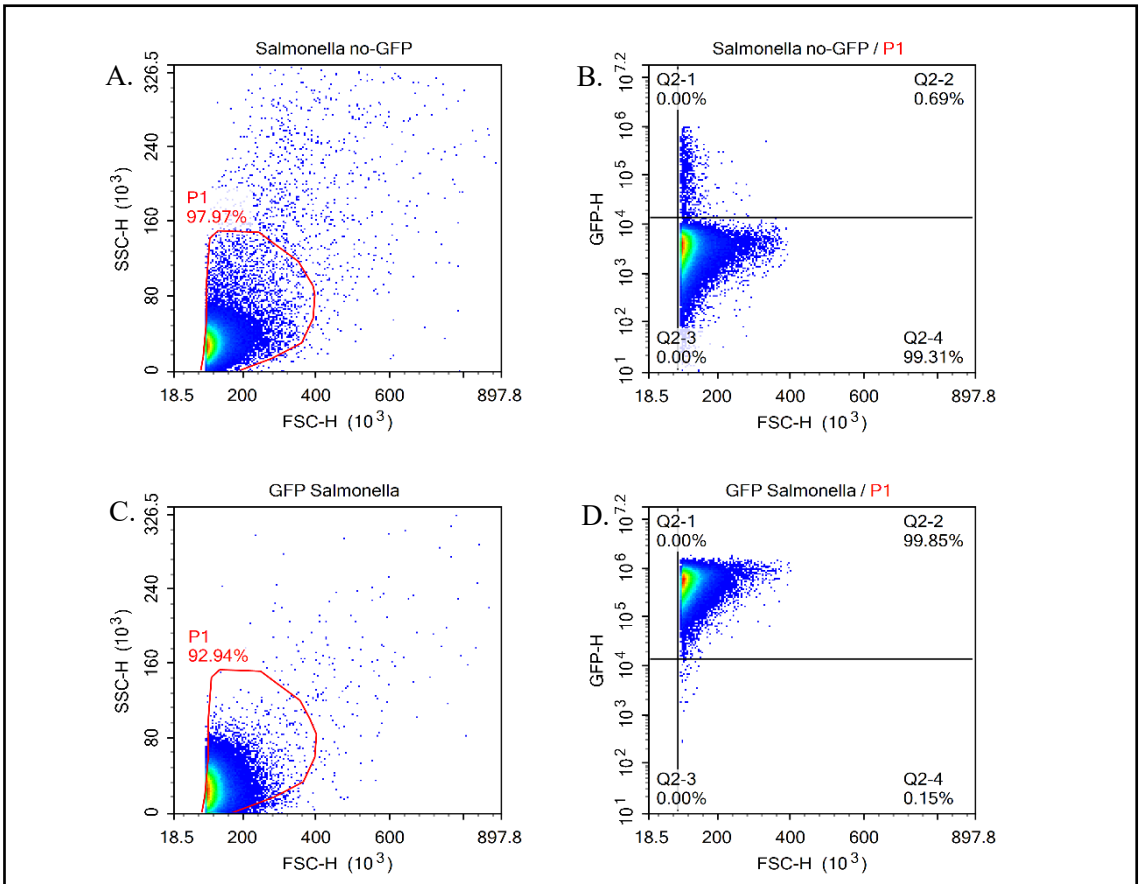

Figure 4: The first two graphs (A & B) show the flowcytometry results for *Salmonella* (SL1344) without a GFP plasmid. The bottom graphs (C & D) represent the flowcytometry results for *Salmonella* (SL1344-GFP) transformed with a GFP plasmid.

4.2 Optimisation of multiplicity of infection (MOI) value for salmonellosis.

For the optimisation of salmonellosis, RAW264.7 cells were infected with different MOI values, which has been done in singlets multiple times. The percentages of FSC/SSC ranged from 26,98% to 67,89% in all conditions (UI, MOI 1, MOI 10, MOI 100) in all time points. These percentages stand for the cells inside the gating that was set to represent the cells in question or the good-looking population. The results for each condition are presented in (Figure 5, A) in which the mean value for all FSC/SSC values was 56,4%. (Figure 5, B) presents the GFP signal percentage in all conditions and timepoints. For uninfected cells, their GFP signal each timepoint was (0,28, 0,29, 0,23, 0,05) respectively. For MOI 1, the values were (0,33, 0,28, 0,25, 0,12) respectively. As for MOI 10, the values were (0,92, 0,98, 0,54, 0,23) in order of timepoints. Last is MOI 100, which showed the most increase in GFP signal compared to MOI 1 and MOI 10, the values respectively were (7,38, 6,73, 4,13, 1,42). Each MOI value showed a trend that was represented by a peak of GFP signal at 30 min and it decreased gradually through the timepoints and when it reached 24 hours, it became almost invisible. Going back to (Figure 5, A & B), those graphs represent uninfected and uninfected FSC/SSC and GFP signal percentages. And when comparing graph A and B, graph B shows a distinct population above threshold that was set using the uninfected cells, therefore, at this point with only infections, GFP signal is easily distinguished.

Figure 5.A

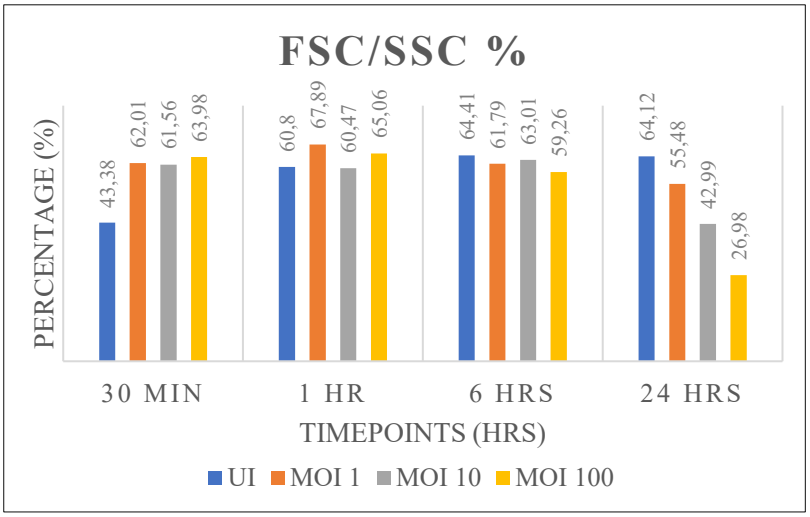

Figure 5.B

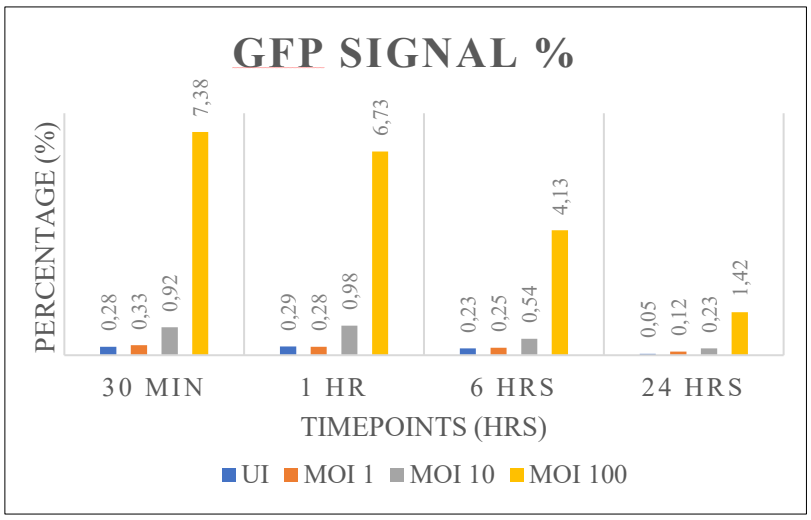

Figure 5: Graph (A) shows the forward and side scatter percentage for different MOI values for salmonellosis in 4 timepoints. Graph (B) shows the GFP signal in percentages for different MOI values in 4 timepoints.

4.3 PARP inhibitor PJ34 optimisation and autofluorescence

To optimise the right concentration to use to treat cells with PJ34 during salmonellosis, the right concentration of PJ34 that can be used without causing any interference with the GFP signal. This experiment has been done twice; the first time included treating RAW264.7 cells with 10 concentrations of PJ34 ranging from 0 to 100 µM for 24 hours and then scraped the cells and analysed them with all the detectors in the flow cytometer. (Figure 6, A) Although most of the other lasers showed an increase of signal with the increase of concentration, the only signal of interest is the GFP signal, which showed an increase in signal after 50 µM. To narrow the search, the second experiment was done to only detect the GFP signal. The cells were treated with 4 concentrations of PJ34 for 4 and 24 hours. The cells were scraped at 4 hours and analysed with the flow cytometer and the same thing was done at 24 hours. (Figure 6, B) There was no distinguishable difference between 4 hours and 24 hours, but similar to graph (A), there was an increase in the GFP signal above 50 µM of PJ34 in both timepoints, and as a result of that, it was preferred to use concentrations under 50 µM of PJ34 so that the GFP signal of PJ34 does not interfere with the GFP signal of salmonella during infections. The reason behind the intrinsic GFP signal that took place when increasing the concentration of PJ34 is yet to be known, it could be due to the presence of a benzene ring, which could have caused the autofluorescence or due to a reaction that took place during the 4- or 24-hour time periods.

A.

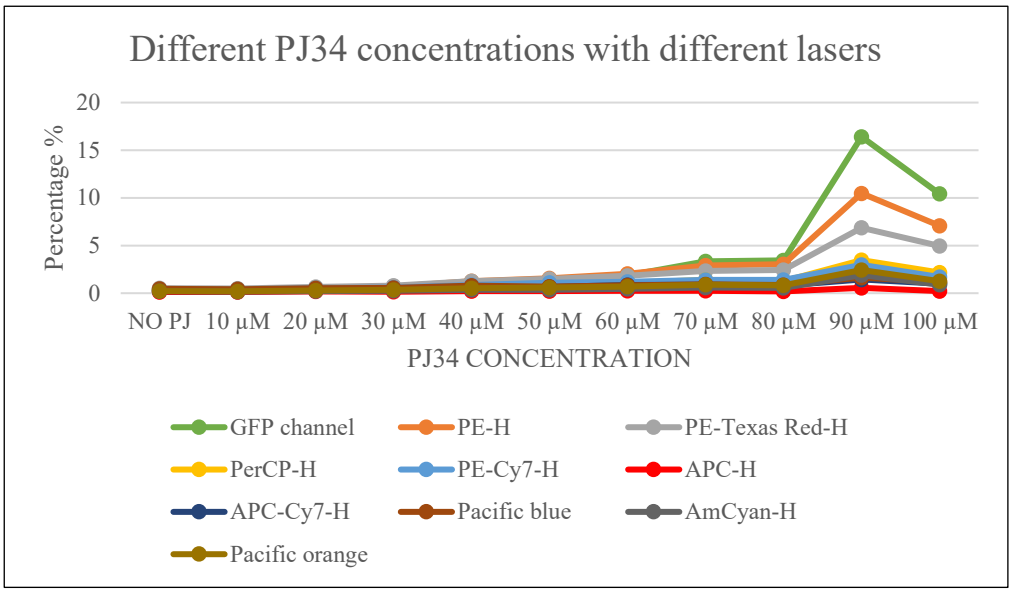

B.

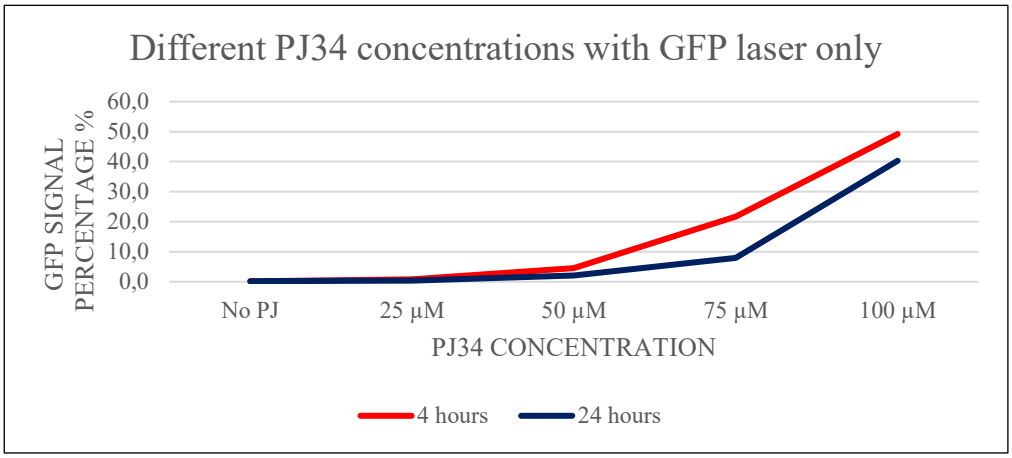

Figure 6: Prior to using PJ34 for infections, it has been tested using different wavelengths with flow cytometry. (A) shows signals of 10 different lasers using RAW264.7 cells treated with PJ34 for 24 hours. (B) shows the GFP signal emission only in cells treated with PJ34 for 4 hours and 24 hours using flow cytometry.

4.4 PJ34 treatment showed more cells associated with bacteria than non-treated cells at 6 hours.

In order to study the significance of ADP-ribosylation to salmonellosis, the PARP inhibitor PJ34 was used, and based on the PJ34 value optimisation experiment, it has been decided to experiment with 25 µM and 50 µM PJ34. The cells were treated prior to infection for 4 hours with the said concentrations of PJ34. The cells were then infected with *Salmonella*-GFP and left to incubate. The cells were then scraped at each time point (30 min, 1 hr, 6 hrs, 24 hours) and analysed using flow cytometry. Keep in mind that during all time points, PJ34 was included in the fresh media added to the cell culture. The

control here was uninfected RAW264.7 cells and RAW264.7 infected with *Salmonella*-GFP with no PJ34. The second set contained RAW264.7 cells infected with *Salmonella*-GFP and was treated with 25 μM of PJ34. The last set had RAW264.7 cells that were infected with *Salmonella*-GFP and was treated with 50 μM of PJ34. The same trend visualised in previous infection experiments was found in this experiment, which is demonstrated by an increase in GFP signal at 30 minutes and a gradual decrease in it through the 24 hours. (Figure 7) When comparing infected cells and infected cells that were treated with 25 μM of PJ34, it is clear that there are more cells associated with bacteria in the PJ34 treated cells than the infected cells with no PJ34 treatment at 6 hours. For infected cells and 50 μM of PJ34, there has also been an increase in cells associated with bacteria during 6 hours of infection. To further study this phenomenon and to know whether this difference between the control and PJ34 treated is significant and can prove that ADP-ribosylation does indeed have a significant effect over salmonellosis, a T-test was performed to compare between infected (I) and infected plus 25 μM of PJ34 (I + 25 μM) and another T-test to compare between (I) and infected plus 50 μM of PJ34 (I + 50 μM). For the first T-test for (I) and (I + 25 μM), the p-value acquired was 0.386225938, indicating that the p-value > 0.05 and that the difference visualised in the graph is not significant. As for the second T-test for (I) and (I + 50 μM), the p-value was 0.167062892, indicating that the p-value > 0.05, which in turn also means that the difference visualized between these two groups is not significant. In conclusion, it can only be said that PJ34 has no major effect on salmonellosis.

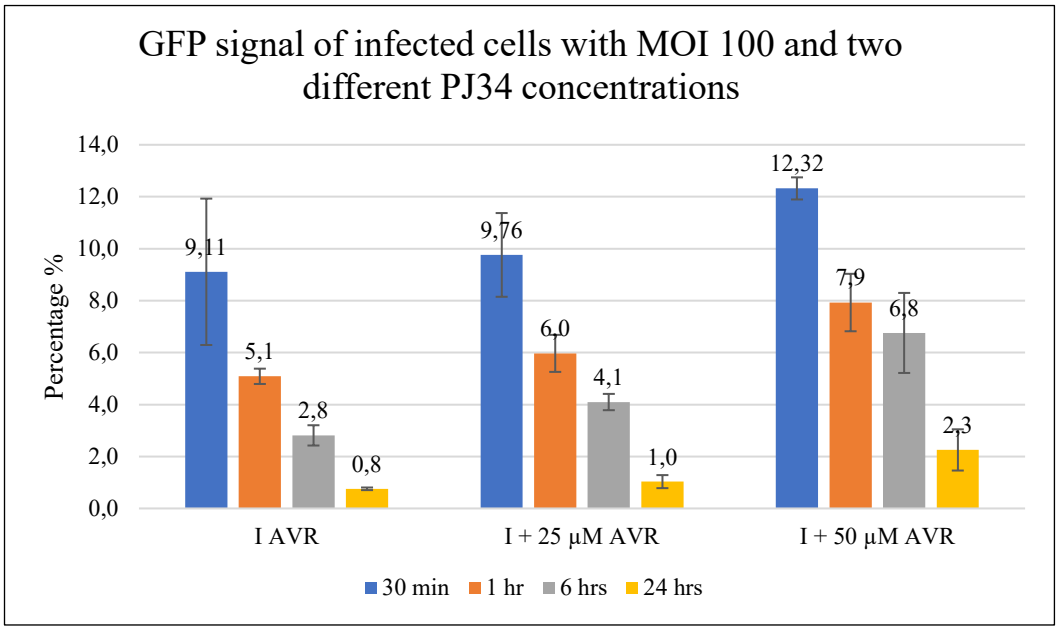

Figure 7: This graph shows the *Salmonella*-GFP signal in RAW264.7 cells infected with an MOI value of 100 and treated with 25 µM and 50 µM of PJ34. This experiment was done in triplicates and the mean value was generated and a standard deviation bar was used to show the difference between the values.

4.5 Heterogenous nature of infection characterised by the different number of bacteria per infected cell using epifluorescence microscopy.

To get a closer look at *Salmonella*-macrophage interaction during salmonellosis, an imaging technique was applied. The cells were seeded in a 24 well plates containing cover slips, which were then transferred onto a slide after infection, fixation, and staining. Epifluorescence microscopy was the imaging technique of choice in this experiment since it provides the basic information needed for a peek at the interaction between *Salmonella* and RAW264.7 cells. The magnification used was 63x oil immersion lens and the images acquired were in grey scale and a colour filter in the program used was applied to the green channel for the GFP-signal (*Salmonella*) and for the blue channel for the macrophage nuclei stained with DAPI. The cells were treated with 20 µM of PJ34 and incubated before infections. The controls included uninfected and also infected with *Salmonella* with MOI 20. The previous experiments were done by one of the research group teammates. The time points chosen for this experiment were 1 hour, 6 hours, 12 hours, and 24 hours. Around 50 images were generated for each category in each time point. For every category, 100 cells were counted manually, and for every one of those

cells, the number of bacteria attached to it was counted too. In order to facilitate the counting process, those 100 cells were further categorised into cells that contained zero bacteria, 1-3 bacteria, 4-8 bacteria, 9-12 bacteria, and more than 12 bacteria per cell. (Figure 9) For the first hour, when comparing infected cells and cells that are infected and were treated with PJ34, there were less cells associated with bacteria for both (I) and (I-PJ) and only 13 to 14 cells had 1-3 bacteria per cells. After 6 hours of infection, there were still many cells that were not infected, yet heavier infections were visualised compared to the first hour. Around 35 cells were not infected for both (I) and (I-PJ), and from here, a slight difference between (I) and (I-PJ) is becoming visible in which (I) showed 8 cells that were infected with 1-3 bacteria and 11 cells infected with 1-3 bacteria for (I-PJ). For 4-8 bacteria per cell, (I) had more than (I-PJ), with similar values for 9-12 bacteria per cell. Only (I-PJ) showed heavily infected cells at 6 hours (>12 bacteria per cell). At 12 hours, the number of bacteria seemed to go down slight in (I) for all categories, yet for (I-PJ), the infection seemed to persist, and the number of bacteria has risen slightly. After 24 hours of infection, the infected cells that did not contain PJ34 seemed to have almost cleared out the infected with over 40 cells that were infected and the rest with lightly infected or contained debris. For infected cells that contained PJ34, the process of getting rid of the bacteria was going slower with only 39 cells were cleared and the rest contained over 1 to 8 bacteria per cell. Figure 8 shows the workflow of the macro used for this experiment.

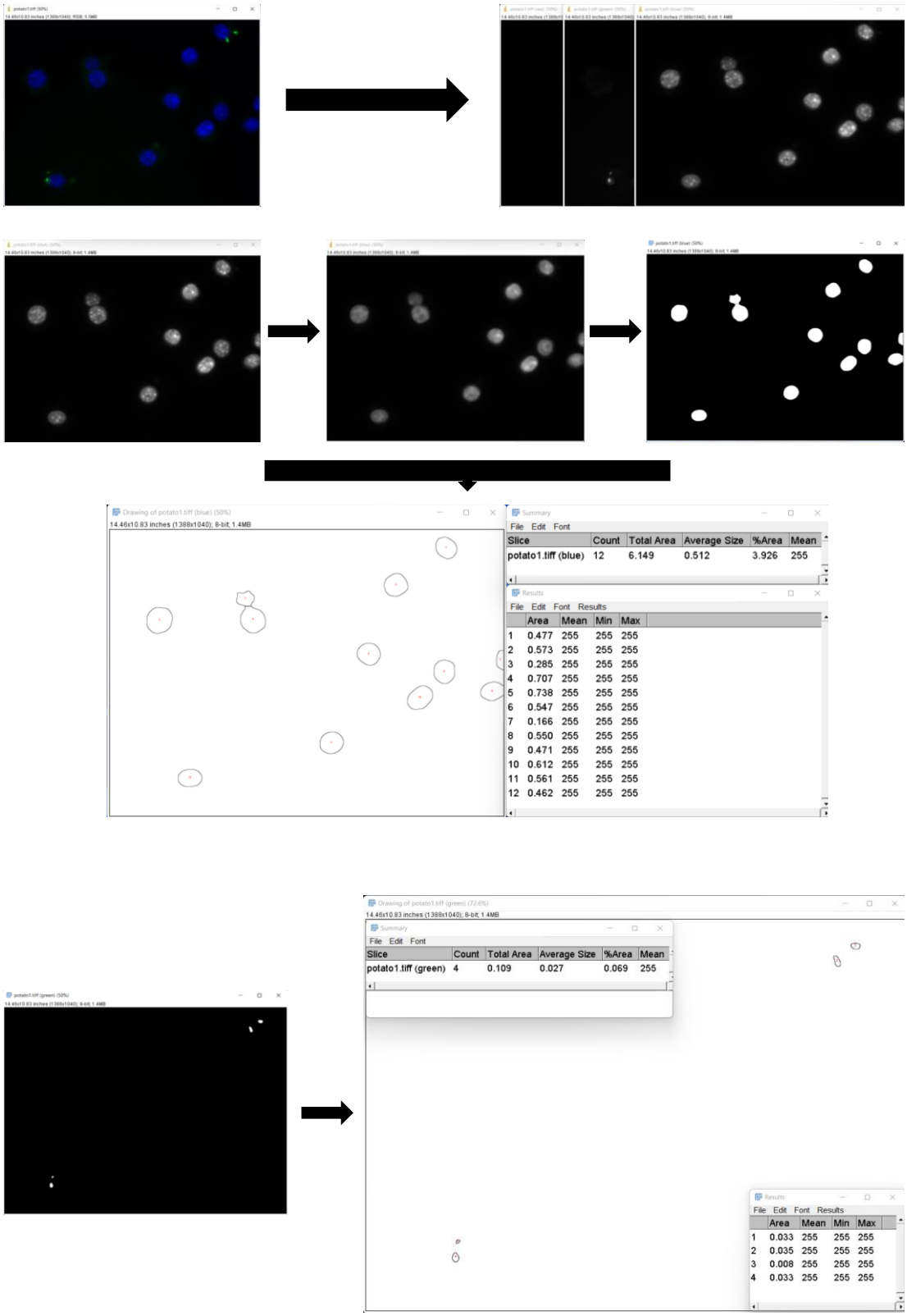

Figure 8: The RGB image is split into 3 images. The macro starts working on the blue channel where it blurs the image, threshold it, watershed and then count the number of nuclei detected and a table is generated and saved. The macro then opens the green channel, thresholds it and counts the bacteria and generates a table with the information needed.

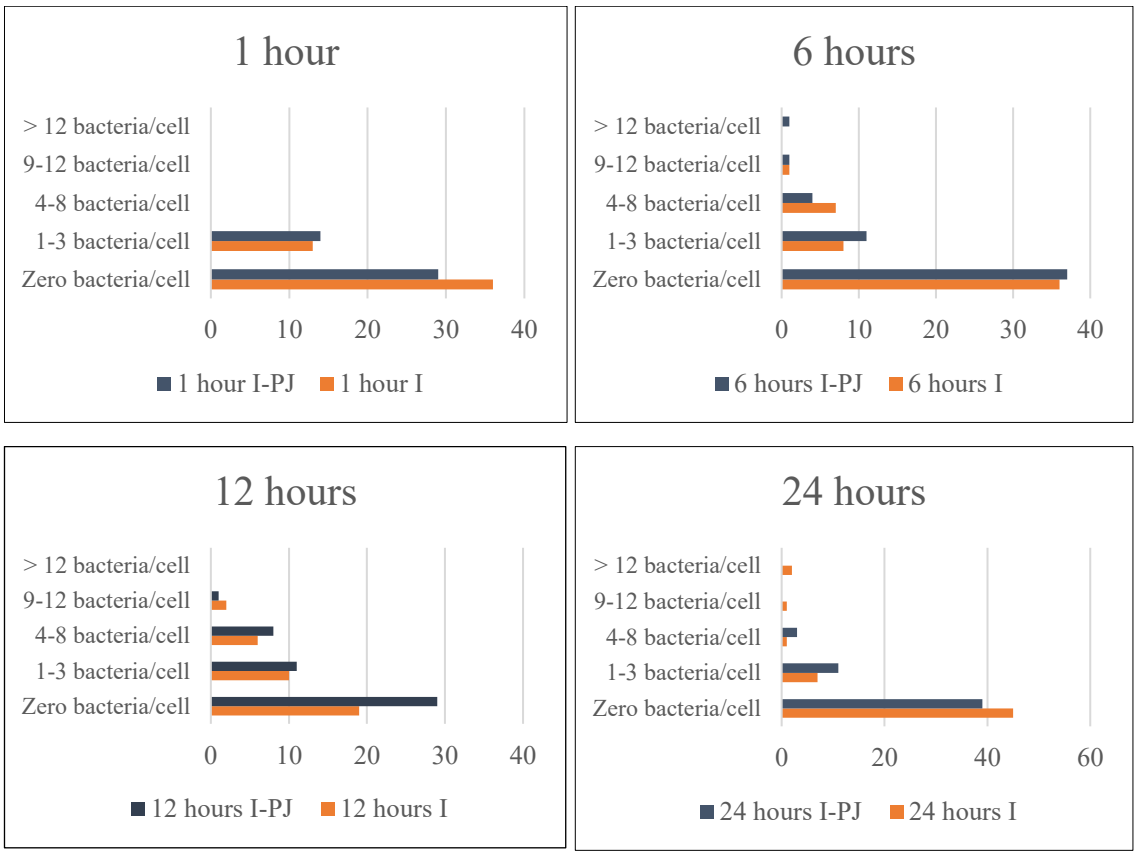

Figure 9: This figure shows the number bacteria per cell for 4 different time points. A number of 50 cells were counted for each time point and for each cell, the number of bacteria were calculated too, and graphs were made based on how many bacteria are within the cells for both infected (I) and for infected + PJ34 (I-PJ)

5. Discussion

Bacteria are microorganisms that play important roles in health and disease, serving as essential structural systems for understanding molecular mechanisms and developing new biotechnological methods. (Kapanidis et al., 2018) Bacteria have evolved complicated, multicomponent cellular machinery to perform key biological functions such cell division/separation, motility, protein secretion, DNA transcription/replication, and conjugation/competence. (Cattoni et al., 2012) Due to that, the need for single cell imaging has increase to further understand the heterogenous processes that take place within bacteria and during bacterial infections. It is important to explicate how cells develop and coordinate processes in order to gain a systems-level understanding of cellular growth, structure, and function. (Huang, 2015) . By counting molecules, characterising their intracellular location and mobility, and identifying functionally different molecular distributions, this toolbox allows in vivo quantitative biology to be used. Importantly, all of this can be done while imaging vast populations of cells, allowing for thorough views of bacterial community heterogeneity. (Kapanidis et al., 2018)

In this research, an MOI value of 100 was used in order to study *Salmonella* at a single cell resolution since going below that would not show what goes on during infection. In 2012, an experiment was done to study the dynamics of *Salmonella* infection at the single cell level, in which they performed experiments with increasing MOI values and found that only at extreme MOI values, almost all of the cell in the culture would be infected. For example, an MOI of 800, 1483 out of 1500 cells were infected with *Salmonella*, but throughout their experiments, they chose to use an MOI value of 50 to study whether reinfection of the same cell occurs and might influence the number of bacteria within the cell. The imaging technique used there was real-time confocal microscopy of individual cells, and then calculated the probability of reinfection. (Gog et al., 2012) Single-molecule imaging techniques have significantly improved our understanding of bacterial cell functions in recent years. They have changed our understanding of the kinetics, heterogeneity, and reaction pathways in many fundamental biological systems. They have the ability to go beyond ensemble averages, allowing for direct detection of heterogeneity within molecular populations. (Kapanidis et al., 2018) A resolution of 20 nm can now be reached inside single living cells using single fluorescent molecules to overcome the optical microscopy barrier, a spatial domain previously only attainable by electron microscopy. A single bacterial protein complex can

be tracked as it performs its functions and elaborate cellular structures can be observed as they migrate and reorganise during the cell cycle. (Kapanidis et al., 2018)

Bacterial pathogens infect mammalian host cells in dynamic processes that have evolved extensively, allowing them to modify the cellular functions using sophisticated mechanisms of action. (Kommnick et al., 2019) They may colonise extracellular niches, adhere to epithelial cell surfaces, overcome host barriers, establish intracellular infections, or employ a combination of these strategies during the infection process. (Park et al., 2021) A variety of imaging techniques can be used to visualise epithelial cells, *in vitro* infection models and host-pathogen interactions. In regards of this experiment, epifluorescence microscopy was used to acquire images of salmonellosis at a magnification of 60X. Higher-resolution light microscopy techniques, including epifluorescence microscopy and CLSM, allow imaging of bacterial colonisation of epithelial cell layers, bacterial internalisation, and bacterial subcellular localisation within epithelial cells reaching a resolution of 1 µm. Lower resolution light microscopy techniques including brightfield, phase contract, and differential interference contrast (DIC) imaging can be used to investigate epithelial cell layer integrity and differentiation at a resolution of 100 µm to 10 µm. More precise colocalization experiments can be done using super resolution microscopy that can track proteins at a resolution of 0.1 µm. Toxins, transcriptional regulators, and immuno-regulatory chemical localization inside host subcellular niches can be studied using electron microscopy, allowing insight into host-pathogen interactions at a resolution as high as 0.005 µm. (Park et al., 2021)

Infectious diseases are the second leading cause of death worldwide. (Lozano et al., 2012) In managing the burden of those infections, public health initiatives are only partially successful. There is still a lack of effective vaccinations for important infections, and the steep fall in the discovery of new antibiotics over the past 20 years, combined with the sharp rise in antibiotic resistance, has drastically reduced the number of treatment options. (Bumann, 2019) One example of such infectious diseases are systemic *Salmonella* infections, which are becoming a leading cause of death worldwide and are getting harder to cure. (Bumann, 2019) Human typhoid fever is caused by *S.Typhi*, which is responsible for an estimated 21 million cases worldwide each year, and even after antibiotic therapy, 15% of persons treated for typhoid fever relapse, and 1-6% of infected people become symptomless, chronic carriers or operate as reservoirs for the disease. (Fisher et al., 2016) Recent single-cell findings from a mouse model of typhoid fever demonstrate that while some *Salmonella* cells are eliminated by the host immune system,

other *Salmonella* cells continue to grow in the same tissue, progressing the fatal disease. The *Salmonella* cells that are still alive have extremely heterogenous growth rates, metabolisms, and stress levels. (Bumann, 2019) Those non-growing *Salmonella* persisters reprogram macrophages using effectors secreted by SPI-2 and SPI-3 that dampen the proinflammatory innate immune responses and induces anti-inflammatory macrophage polarisation. (Fisher et al., 2018)

ADP-ribosylation is well-known to play a crucial role in numerous host-pathogen interactions. Many major bacterial toxins are ARTs, including *E. coli*, *P. aeruginosa*, *C. botulinum*, *S. aureus*, and *V. cholera*. Those bacteria encode for ARTs that target proteins like actin, Rho GTPases, and elongation factor 2 that cause cell death. (Fehr et al., 2020) For *Salmonella*, its ADP-ribosylating toxin in spvB, which is secreted into the host cytoplasm through SPI-2 T3SS. It works on ADP-ribosylating actin monomers, preventing their polymerisation. (Cheng and Wiedmann, 2019) Practically all research on the role of mammalian PARPs in acute and chronic bacterial infections has focused on PARP1. Research has demonstrated that the lack of PARP1 delays the immune system's proinflammatory response in a mouse model of oral S. typhi. Many of the PARP1-dependent genes were known immune response genes, notably those linked to IFN-signalling. This finding suggests that PARP1 may be involved in the recruitment of immune cells during salmonellosis. (Miettinen et al., 2019) PJ34, a PARP1 and PARP2 inhibitor was used to visualise the importance of ADP ribosylation to salmonellosis. It was clear that when inhibiting the ADP-ribosylation process during salmonellosis and analysing the cells using flowcytometry during each time point, there was a slight increase in RAW264.7 cells associated with *Salmonella* and the infection were resolving rather slower than the infections that were going on normally without PJ34. Yet, the statistical analysis revealed that that slight increase was not significant and not enough to say that ADP-ribosylation has a major effect on salmonellosis. When performing the same experiment on coverslips in order to acquire images using epifluorescence microscopy, the same trend seen with flowcytometry was seen in the images, but not enough images were taken to give the same conclusion as the flowcytometry experiment, but it confirmed that salmonellosis has a heterogenous nature since the images acquired showed that the cells were infected with a different number of bacteria. In ongoing research in the host laboratory, PARP14 was found to be upregulated during salmonellosis. Upon stimulation of murine macrophages by a toxin, numerous Parp genes transcription was dynamically controlled. Multiple inflammatory stimuli induced PARP14, which then translocated into

the nucleus of stimulated cells. Because PARP14 was necessary for the nuclear accumulation of a number of IFN-stimulated gene (ISG)-encoded proteins, quantitative mass spectrometry analysis revealed that PARP14 bound to these proteins and inhibited their ability to proliferate in murine macrophages, also revealing PARP14 inhibited *S. typhimurium* growth in murine macrophages. (Caprara et al., 2018) Other in vitro studies have shown that PARP14 inhibits proinflammatory IFN–STAT1 signalling and stimulates the anti-inflammatory IL-4-STAT6 pathway in primary human macrophages. (Fehr et al., 2020) PARP14-deficient RAW264.7 macrophages had more viable intracellular Salmonella, implying that the presence of PARP-14 inhibits *Salmonella* growth in macrophages. (Caprara et al., 2018) According to the previously mentioned literature and ongoing research, it was hypothesised that PARP14 might have a direct effect on salmonellosis but the functional importance of PARP-14 and its mechanism of action in salmonellosis are yet to be revealed.

Combining mouse models, *in vivo*, *ex vivo* and *in vitro* imaging techniques and molecular testing would give great insight into the host-pathogen interaction at a single cell resolution and a molecular level if advanced imaging techniques were used. This would enable to a further understanding of the pathogenesis of pathogens, in this case *Salmonella*, leading to the discovery of more specific and advanced treatment options for persistent and chronic infections.

6. Conclusion

In conclusion, according to the results acquired through this research, using a high MOI is better suited for studying *Salmonella* at a single-cell level. Using MOI 100 showed the nature of salmonellosis during a timeline of 24 hours. In regards of ADP ribosylation, using a concentration higher than 50 μM of PJ34 might interfere with the results due to intrinsic fluorescence or product fluorescence that was a result of a reaction taking place during PJ34 treatment. After treating the cells with the suitable PJ34 concentrations, it was found that it has no major effect on salmonellosis, but according to the image analysis done on the images acquired with epifluorescence microscopy, it was clear that cells were getting infected with a different number of bacteria hence confirming the heterogeneity of salmonellosis. In order to further study the functional importance of ADP-ribosylation to salmonellosis, experiments with other pharmaceutical PARP inhibitors should be conducted. The use of PARP-14 knockdown RAW264.7 macrophages and PARP-14 knockout mice would also shine light on the importance of PARP-14 and what is has to do with salmonellosis. Regarding the imaging techniques used, a larger number of images should be acquired in future experiments and the efficiency and accuracy of the image analysis macro should be improved. Better understanding of the pathogenesis of salmonellosis would open a new door in therapeutics and would give a better understanding of PARPs and their significance in the human body and their importance for infections.

7. Acknowledgements

I would like to acknowledge and give my warmest thanks to my supervisor Arto Pulliainen and my mentor Madhukar Vendantham who made this work possible. Their guidance and advice carried me through all the stages of my thesis. I would also like to thank my research group members who also taught me and gave me advice when I was working on my experiments. They were patient and taught me many skills that I will carry with me through out my career. I would also like to give special thanks to my best friends and my family as a whole for their continuous support and understanding when I was working on my thesis project and writing it. Pushing me through tough times and believing in me are what made reach the finish line. Last but not least, I would like to thank my program coordinators and BIMA teachers for teaching me, believing in me and being my friends when I needed one throughout my degree, I would not have succeeded without having a good support team behind me.

Appendix

Automated Image analysis in ImageJ

1. Primarily, when we run the program, this part of the code will show a window that will ask for an input directory and output directory. The input needed should contain “tiff” suffix in order to be opened for image analysis.

```
#@ File (label = "Input directory", style = "directory")
input
#@ File (label = "Output directory", style = "directory")
output
#@ String (label = "File suffix", value = ".tiff") suffix
```

2. In order to be able to open the file and obtain the name of it and keep it throughout the analysis, this part of the code will process the file, open it, acquire its name and make a list of the images that will be analysed.

```
processFolder(input);
function processFolder(input) {
     list = getFileList(input);
     list = Array.sort(list);
     for (i = 0; i < list.length; i++) {
          if(File.isDirectory(input
+File.separator+list[i]))
               processFolder(input
+File.separator+list[i]);
          if(endsWith(list[i], suffix))
               processFile(input, output, list[i]);
     }
}
```

3. At this stage, all unnecessary files will be closed and the image we need is opened. Since the images we have multi-channel images, our first step is splitting the images into red, green and blue images (RGB channels). Our images contain DAPI (which emits blue fluorescence) and GFP (green fluorescent protein) from *Salmonella*. The title of the image is acquired for further analysis.

```
function processFile(input, output, file) {
    run("Close All"); //to close any unnecessary windows
    open(file);
    run("Split Channels");
    titlelist=getList("image.titles");
    title=titlelist[2];
```

4. When the title is acquired, analysis for the blue channel will start. At this stage, the image is 8-bit, which means it is in grey scale. In order to remove any noise caused by the staining process, a blurring process is done, and the one used here is the median. The science behind this is that there will be a 9 2D kernel that will pass through the pixels in the images and takes the median of the pixel intensities, thus giving us a less noisy image at the end. This step is followed by thresholding by making the images binary, and it very much dependant on the person doing it because every person would threshold differently, but it is always important to keep the histogram in mind so that we do not lose any important pixels. ImageJ already has some built in thresholding programs that could work but it is fine to do it manually by following increasing or decreasing the white and black pixels in a way that does not change the general image. This step might remove the separations between neighbouring cells and makes it hard to distinguish between them and the program might count them as one cell, so I added another step called watershed, that adds lines between neighbouring cells. Then particle analysis is done by setting a threshold for the size we need and the circularity so that we only calculate the number of nuclei and it would ignore any small particles that might have resulted from the thresholding. It will finally display a summary table with the number of nuclei in the image.

```
    selectWindow(title); //first image from the already
split channel representing the blue channel
```

```
run("Median...", "radius=10");
run("Gray Morphology", "radius=4 type=circle operator=erode");
setAutoThreshold("Default dark");
//setThreshold(38, 255);
setOption("BlackBackground", true);
run("Convert to Mask");
run("Watershed"); //to separate the particles and show every cell as individual
run("Analyze Particles...", "size=100-Infinity pixel circularity=0.00-5.00 show=Outlines display clear include summarize");
run("Close");
//close(title)
```

5. The program switched to the second image since the first one was closed and then proceed to thresholding. I did not blur images here because the bacteria are very small, and data might be lost during blurring. Then watershed is done to separate close bacteria (a spot for error here). This is followed by particle analysis with a different size and circularity than the nuclei.

```
title2=titlelist[1];
print(title2);
selectWindow(title2);
setAutoThreshold("MaxEntropy dark no-reset");
//run("Threshold...");
//setThreshold(51, 255);
setOption("BlackBackground", true);
run("Convert to Mask");
```

```
    run("Watershed");

    run("Analyze Particles...", "size=10-Infinity pixel
circularity=0.00-1.00 show=Outlines display clear include
summarize");

    close();
```

6. And finally, the file is saved as a .txt file called summary in the output directory selected at the beginning of the macro.

```
    Table.save(output+"/Summary.txt","Summary");

    print("Processing: " + input + File.separator + file);

    print("Saving to: " + output);

    run("Close All");


}
```

References

Antoniou, A.N., S.J. Powis, and J. Kriston-Vizi. 2019. High-content screening image dataset and quantitative image analysis of Salmonella infected human cells. *BMC Research Notes*. 12:1–4. doi:10.1186/s13104-019-4844-5.

Balasubramanian, R., J. Im, J.S. Lee, H.J. Jeon, O.D. Mogeni, J.H. Kim, R. Rakotozandrindrainy, S. Baker, and F. Marks. 2019. The global burden and epidemiology of invasive non-typhoidal Salmonella infections. *Human Vaccines and Immunotherapeutics*. 15:1421–1426. doi:10.1080/21645515.2018.1504717.

Bergeron, J.R.C., L.J. Worrall, N.G. Sgourakis, F. DiMaio, R.A. Pfuetzner, H.B. Felise, M. Vuckovic, A.C. Yu, S.I. Miller, D. Baker, and N.C.J. Strynadka. 2013. A Refined Model of the Prototypical Salmonella SPI-1 T3SS Basal Body Reveals the Molecular Basis for Its Assembly. *PLoS Pathogens*. 9. doi:10.1371/journal.ppat.1003307.

Brauner, A., O. Fridman, O. Gefen, and N.Q. Balaban. 2016. Distinguishing between resistance, tolerance and persistence to antibiotic treatment. *Nature Reviews Microbiology*. 14:320–330. doi:10.1038/nrmicro.2016.34.

Brodsky, I.E. 2020. JAK-ing into M1/M2 Polarization SteErs Salmonella-Containing Macrophages Away from Immune Attack to Promote Bacterial Persistence. *Cell Host and Microbe*. 27:3–5. doi:10.1016/j.chom.2019.12.007.

Bumann, D. 2019. Salmonella Single-Cell Metabolism and Stress Responses in Complex Host Tissues . *Microbiology Spectrum*. 7. doi:10.1128/microbiolspec.bai-0009-2019.

Bumann, D., and O. Cunrath. 2017. Heterogeneity of Salmonella -host interactions in infected host tissues. *Current Opinion in Microbiology*. 39:57–63. doi:10.1016/j.mib.2017.09.008.

Caprara, G., E. Prosperini, V. Piccolo, G. Sigismondo, A. Melacarne, A. Cuomo, M. Boothby, M. Rescigno, T. Bonaldi, and G. Natoli. 2018. PARP14 Controls the Nuclear Accumulation of a Subset of Type I IFN–Inducible Proteins. *The Journal of Immunology*. 200:2439–2454. doi:10.4049/jimmunol.1701117.

Carina Kommnick, M.H. 2021. Correlative Light and Scanning Electron Microscopy to Study Interactions of Salmonella enterica with Polarized Epithelial Cell Monolayers. *Methods in Molecular Biology*. 2182.

Cattoni, D.I., J.B. Fiche, and M. Nöllmann. 2012. Single-molecule super-resolution imaging in bacteria. *Current Opinion in Microbiology*. 15:758–763. doi:10.1016/j.mib.2012.10.007.

Chen, J., and B. Park. 2018. Label-free screening of foodborne Salmonella using surface plasmon resonance imaging. *Analytical and Bioanalytical Chemistry*. 410:5455–5464. doi:10.1007/s00216-017-0810-z.

Cheng, R.A., and M. Wiedmann. 2019. The ADP-ribosylating toxins of Salmonella. *Toxins (Basel)*. 11. doi:10.3390/toxins11070416.

Cho, S.H., S. Goenka, T. Henttinen, P. Gudapati, A. Reinikainen, C.M. Eischen, R. Lahesmaa, and M. Boothby. 2009. PARP-14, a member of the B aggressive lymphoma family, transduces survival signals in primary B cells. *Blood*. 113:2416–2425. doi:10.1182/blood-2008-03-144121.

Crawford, K., J.J. Bonfiglio, A. Mikoč, I. Matic, and I. Ahel. 2018. Specificity of reversible ADP-ribosylation and regulation of cellular processes. *Critical Reviews in Biochemistry and Molecular Biology*. 53:64–82. doi:10.1080/10409238.2017.1394265.

Crump, J.A., M. Sjölund-Karlsson, M.A. Gordon, and C.M. Parry. 2015. Epidemiology, clinical presentation, laboratory diagnosis, antimicrobial resistance, and antimicrobial management of invasive Salmonella infections. *Clinical Microbiology Reviews*. 28:901–937. doi:10.1128/CMR.00002-15.

Deborah A. Adams1; Kimberly R. Thomas, M.R.A.J.D.L.F.M.G.B.M.P.S.D.H.O.A.W.S.W.J.A. 2015. Summary of Notifiable Infectious Diseases and Conditions — United States, 2015.

van Engelenburg, S.B., and A.E. Palmer. 2010. Imaging type-III secretion reveals dynamics and spatial segregation of Salmonella effectors. *Nature Methods*. 7:325–330. doi:10.1038/nmeth.1437.

Fehr, A.R., S.A. Singh, C.M. Kerr, S. Mukai, H. Higashi, and M. Aikawa. 2020. The impact of PARPs and ADP-ribosylation on inflammation and host-pathogen interactions. *Genes and Development*. 34:341–359. doi:10.1101/gad.334425.119.

Felgner, S., I. Spöring, V. Pawar, D. Kocijancic, M. Preusse, C. Falk, M. Rohde, S. Häussler, S. Weiss, and M. Erhardt. 2020. The immunogenic potential of bacterial flagella for Salmonella-mediated tumor therapy. *International Journal of Cancer*. 147:448–460. doi:10.1002/ijc.32807.

Fernandes, E., V.C. Martins, C. Nóbrega, C.M. Carvalho, F.A. Cardoso, S. Cardoso, J. Dias, D. Deng, L.D. Kluskens, P.P. Freitas, and J. Azeredo. 2014. A bacteriophage detection tool for viability assessment of Salmonella cells. *Biosensors and Bioelectronics*. 52:239–246. doi:10.1016/j.bios.2013.08.053.

Fisher, R.A., A.M. Cheverton, and S. Helaine. 2016. Analysis of Macrophage-Induced Salmonella Persisters. 1333:177–187. doi:10.1007/978-1-4939-2854-5.

Fisher, R.A., B. Gollan, and S. Helaine. 2017. Persistent bacterial infections and persister cells. *Nature Reviews Microbiology*. 15:453–464. doi:10.1038/nrmicro.2017.42.

Fisher, R.A., T.L. Thurston, A. Saliba, I. Blommestein, J. Vogel, and S. Helaine. 2018. Salmonella persisters undermine host immune defenses during antibiotic treatment. 1160:1156–1160.

Goenka, S., and M. Boothby. 2006. Selective potentiation of Stat-dependent gene expression by collaborator of Stat6 (CoaSt6), a transcriptional cofactor.

Gog, J.R., A. Murcia, N. Osterman, O. Restif, T.J. McKinley, M. Sheppard, S. Achouri, B. Wei, P. Mastroeni, J.L.N. Wood, D.J. Maskell, P. Cicuta, and C.E. Bryant. 2012. Dynamics of Salmonella infection of macrophages at the single cell level. *Journal of the Royal Society Interface*. 9:2696–2707. doi:10.1098/rsif.2012.0163.

Gogoi, M., M.M. Shreenivas, and D. Chakravortty. 2019. Hoodwinking the Big-Eater to Prosper: The Salmonella -Macrophage Paradigm. *Journal of Innate Immunity*. 11:289–299. doi:10.1159/000490953.

Gollan, B., G. Grabe, C. Michaux, and S. Helaine. 2019. Bacterial persisters and infection: Past, present, and progressing. *Annual Review of Microbiology*. 73:359–385. doi:10.1146/annurev-micro-020518-115650.

Grantcharova, N., V. Peters, C. Monteiro, K. Zakikhany, and U. Römling. 2010. Bistable expression of CsgD in biofilm development of Salmonella enterica serovar typhimurium. *Journal of Bacteriology*. 192:456–466. doi:10.1128/JB.01826-08.

Groslambert, J., E. Prokhorova, and I. Ahel. 2021. ADP-ribosylation of DNA and RNA. *DNA Repair*. 105. doi:10.1016/j.dnarep.2021.103144.

Gutierrez, D.A., L. Valdes, C. Serguera, and M. Llano. 2016. Poly(ADP-ribose) polymerase-1 silences retroviruses independently of viral DNA integration or heterochromatin formation. *Journal of General Virology*. 97:1686–1692. doi:10.1099/jgv.0.000466.

Helaine, S., J.A. Thompson, K.G. Watson, M. Liu, C. Boyle, and D.W. Holden. 2010. Dynamics of intracellular bacterial replication at the single cell level. 107:3746–3751. doi:10.1073/pnas.1000041107.

Henning, R.J., M. Bourgeois, and R.D. Harbison. 2018. Poly(ADP-ribose) Polymerase (PARP) and PARP Inhibitors: Mechanisms of Action and Role in Cardiovascular Disorders. *Cardiovascular Toxicology*. 18:493–506. doi:10.1007/s12012-018-9462-2.

Huang, F.C. 2009. Upregulation of salmonella-induced IL-6 production in caco-2 cells by PJ-34, parp-1 inhibitor: Involvement of PI3K, p38 MAPK, ERK, JNK, and NF- B. *Mediators of Inflammation*. 2009. doi:10.1155/2009/103890.

Huang, K.C. 2015. Applications of imaging for bacterial systems biology. *Current Opinion in Microbiology*. 27:114–120. doi:10.1016/j.mib.2015.08.003.

Huemer, M., S. Mairpady Shambat, S.D. Brugger, and A.S. Zinkernagel. 2020. Antibiotic resistance and persistence—Implications for human health and treatment perspectives. *EMBO Rep*. 21. doi:10.15252/embr.202051034.

Iwata, H., C. Goettsch, A. Sharma, P. Ricchiuto, W.W. bin Goh, A. Halu, I. Yamada, H. Yoshida, T. Hara, M. Wei, N. Inoue, D. Fukuda, A. Mojcher, P.C. Mattson, A.L. Barabási, M. Boothby, E. Aikawa, S.A. Singh, and M. Aikawa. 2016. PARP9 and PARP14 cross-regulate macrophage activation via

STAT1 ADP-ribosylation. *Nature Communications*. 7. doi:10.1038/ncomms12849.

Jajere, S.M. 2019. A review of Salmonella enterica with particular focus on the pathogenicity and virulence factors, host specificity and adaptation and antimicrobial resistance including multidrug resistance. *Veterinary World*. 12:504–521. doi:10.14202/vetworld.2019.504-521.

de Jonge, N., and F.M. Ross. 2011. Electron microscopy of specimens in liquid. *Nature Nanotechnology*. 6:695–704. doi:10.1038/nnano.2011.161.

Kageyama, S., H. Omori, T. Saitoh, T. Sone, J.L. Guan, S. Akira, F. Imamoto, T. Noda, and T. Yoshimori. 2011. The LC3 recruitment mechanism is separate from Atg9L1-dependent membrane formation in the autophagic response against Salmonella. *Molecular Biology of the Cell*. 22:2290–2300. doi:10.1091/mbc.E10-11-0893.

Kapanidis, A.N., A. Lepore, and M. el Karoui. 2018. Rediscovering Bacteria through Single-Molecule Imaging in Living Cells. *Biophysical Journal*. 115:190–202. doi:10.1016/j.bpj.2018.03.028.

Kehl, A., and M. Hensel. 2015. Live cell imaging of intracellular Salmonella Enterica. *Methods in Molecular Biology*. 1225:199–225. doi:10.1007/978-1-4939-1625-2_13.

Knodler, L.A. 2015. Salmonella enterica: Living a double life in epithelial cells. *Current Opinion in Microbiology*. 23:23–31. doi:10.1016/j.mib.2014.10.010.

Knodler, L.A., S.M. Crowley, H.P. Sham, H. Yang, M. Wrande, C. Ma, R.K. Ernst, O. Steele-Mortimer, J. Celli, and B.A. Vallance. 2014a. Noncanonical inflammasome activation of caspase-4/caspase-11 mediates epithelial defenses against enteric bacterial pathogens. *Cell Host and Microbe*. 16:249–256. doi:10.1016/j.chom.2014.07.002.

Knodler, L.A., V. Nair, and O. Steele-Mortimer. 2014b. Quantitative assessment of cytosolic Salmonella in epithelial cells. *PLoS ONE*. 9. doi:10.1371/journal.pone.0084681.

Knodler, L.A., B.A. Vallance, J. Celli, S. Winfree, B. Hansen, M. Montero, and O. Steele-Mortimer. 2010. Dissemination of invasive Salmonella via bacterial-induced extrusion of mucosal epithelia. *Proc Natl Acad Sci U S A*. 107:17733–17738. doi:10.1073/pnas.1006098107.

Kommnick, C., A. Lepper, and M. Hensel. 2019. Correlative light and scanning electron microscopy (CLSEM) for analysis of bacterial infection of polarized epithelial cells. *Sci Rep*. 9:17079. doi:10.1038/s41598-019-53085-6.

Kunze, F.A., M. Bauer, J. Komuczki, M. Lanzinger, K. Gunasekera, A.-K. Hopp, M. Lehmann, B. Becher, A. Müller, and M.O. Hottiger. 2019. ARTD1 in Myeloid Cells Controls the IL-12/18–IFN-γ Axis in a Model of Sterile Sepsis, Chronic Bacterial Infection, and Cancer. *The Journal of Immunology*. 202:1406–1416. doi:10.4049/jimmunol.1801107.

Li, S., Z. Cui, and X. Meng. 2016. Knockdown of PARP-1 inhibits proliferation and ERK signals, increasing drug sensitivity in osteosarcoma U2OS cells. *Oncology Research*. 24:279–286. doi:10.3727/096504016X14666990347554.

Lozano, R., M. Naghavi, S.S. Lim, S.Y. Ahn MPH, M.B. Alvarado, K.G. Andrews MPH, C.B. Atkinson, I.A. Bolliger, D.B. Chou, K.E. Colson BA, A.B. Delossantos, S.D. Dharmaratne MBBS, A.D. Flaxman, R. Lozano, M. Naghavi, K. Foreman, S. Lim, K. Shibuya, V. Aboyans, J. Abraham, T. Adair, R. Aggarwal, S.Y. Ahn, M.A. AlMazroa, M. Alvarado, H. Ross Anderson, L.M. Anderson, K.G. Andrews, C. Atkinson, L.M. Baddour, S. Barker-Collo, D.H. Bartels, M.L. Bell, E.J. Benjamin, D. Bennett, K. Bhalla, B. Bikbov, A. bin Abdulhak, G. Birbeck, F. Blyth, I. Bolliger, S. ane Boufous, C. Bucello, M. Burch, P. Burney, J. Carapetis, H. Chen, D. Chou, S.S. Chugh, L.E. Coff eng, S.D. Colan, S. Colquhoun, K. Ellicott Colson, J. Condon, M.D. Connor, L.T. Cooper, M. Corriere, M. Cortinovis, K. Courville de Vaccaro, W. Couser, B.C. Cowie, M.H. Criqui, M. Cross, K.C. Dabhadkar, N. Dahodwala, D. de Leo, L. Degenhardt, A. Delossantos, J. Denenberg, D.C. des Jarlais, S.D. Dharmaratne, E. Ray Dorsey, T. Driscoll, H. Duber, B. Ebel, P.J. Erwin, P. Espindola, M. Ezzati, V. Feigin, A.D. Flaxman, M.H. Forouzanfar, F.R. Gerry Fowkes, R. Franklin, M. Fransen, M.K. Freeman, S.E. Gabriel, E. Gakidou, F. Gaspari, R.F. Gillum, D. Gonzalez-Medina, Y.A. Halasa, D. Haring, J.E. Harrison, R. Havmoeller, R.J. Hay, B. Hoen, P.J. Hotez, D. Hoy, et al. 2012. Global and regional mortality from 235 causes of death for 20 age groups in 1990 and 2010: a systematic analysis for the Global Burden of Disease Study 2010. 380. 2095-128 pp.

Malik-Kale, P., S. Winfree, and O. Steele-Mortimer. 2012. The bimodal lifestyle of intracellular Salmonella in epithelial cells: Replication in the cytosol obscures defects in vacuolar replication. *PLoS ONE*. 7. doi:10.1371/journal.pone.0038732.

Malt, L.M., C.A. Perrett, S. Humphrey, and M.A. Jepson. 2015. Applications of microscopy in Salmonella Research.

Mekhaeil, M., K.K. Dev, and M.J. Conroy. 2022. Existing Evidence for the Repurposing of PARP-1 Inhibitors in Rare Demyelinating Diseases. *Cancers (Basel)*. 14. doi:10.3390/cancers14030687.

Mellouk, N., A. Weiner, N. Aulner, C. Schmitt, M. Elbaum, S.L. Shorte, A. Danckaert, and J. Enninga. 2014. Shigella subverts the host recycling compartment to rupture its vacuole. *Cell Host and Microbe*. 16:517–530. doi:10.1016/j.chom.2014.09.005.

Michael S Cohen, P.C. 2017. Insights into the biogenesis, function, and regulation of ADP-ribosylation. *Physiol Behav*. 176:139–148. doi:10.1038/nchembio.2568.Insights.

Miettinen, M., M. Vedantham, and A.T. Pulliainen. 2019. Host poly(ADP-ribose) polymerases (PARPs) in acute and chronic bacterial infections. *Microbes and Infection*. 21:423–431. doi:10.1016/j.micinf.2019.06.002.

Mosser, D.M., and J.P. Edwards. 2008. Exploring the full spectrum of macrophage activation. *Nature Reviews Immunology*. 8:958–969. doi:10.1038/nri2448.

Murray, P.J., J.E. Allen, S.K. Biswas, E.A. Fisher, D.W. Gilroy, S. Goerdt, S. Gordon, J.A. Hamilton, L.B. Ivashkiv, T. Lawrence, M. Locati, A. Mantovani, F.O. Martinez, J.L. Mege, D.M. Mosser, G. Natoli, J.P. Saeij, J.L. Schultze, K.A. Shirey, A. Sica, J. Suttles, I. Udalova, J.A. vanGinderachter, S.N. Vogel, and T.A. Wynn. 2014. Macrophage Activation and Polarization: Nomenclature and Experimental Guidelines. *Immunity*. 41:14–20. doi:10.1016/j.immuni.2014.06.008.

Palazzo, L., P. Mikolčević, A. Mikoč, and I. Ahel. 2019. ADP-ribosylation signalling and human disease. *Open Biology*. 9. doi:10.1098/rsob.190041.

Park, A.J., M.A. Wright, E.J. Roach, and C.M. Khursigara. 2021. Imaging host–pathogen interactions using epithelial and bacterial cell infection models. *Journal of Cell Science*. 134. doi:10.1242/jcs.250647.

Peng, Y., Q. Liao, W. Tan, C. Peng, Z. Hu, Y. Chen, Z. Li, J. Li, B. Zhen, W. Zhu, X. Li, Y. Yao, Q. Song, C. Liu, X. Qi, F. He, and H. Pei. 2019. The deubiquitylating enzyme USP15 regulates homologous recombination repair and cancer cell response to PARP inhibitors. *Nature Communications*. 10. doi:10.1038/s41467-019-09232-8.

Perrett, C.A., and M.A. Jepson. 2007. Applications of cell imaging in Salmonella research. *Methods Mol Biol*. 394:235–273. doi:10.1007/978-1-59745-512-1_12.

Picó, Y. 2018. Electron Microscopy Safety Assessment and Migration Tests.

Pradhan, D., and V. Devi Negi. 2019. Stress-induced adaptations in Salmonella: A ground for shaping its pathogenesis. *Microbiological Research*. 229:126311. doi:10.1016/j.micres.2019.126311.

Pucciarelli, M.G., and F. García-del Portillo. 2017. Salmonella Intracellular Lifestyles and Their Impact on Host-to-Host Transmission. *Microbial Transmission*. 95–116. doi:10.1128/microbiolspec.mtbp-0009-2016.

dos Santos, A.M.P., R.G. Ferrari, and C.A. Conte-Junior. 2019. Virulence Factors in Salmonella Typhimurium: The Sagacity of a Bacterium. *Current Microbiology*. 76:762–773. doi:10.1007/s00284-018-1510-4.

Scott, C.C., R.J. Botelho, and S. Grinstein. 2003. Phagosome maturation: A few bugs in the system. *Journal of Membrane Biology*. 193:137–152. doi:10.1007/s00232-002-2008-2.

Sindhwani, A., S.B. Arya, H. Kaur, D. Jagga, A. Tuli, and M. Sharma. 2017. Salmonella exploits the host endolysosomal tethering factor HOPS complex to promote its intravacuolar replication. *PLoS Pathogens*. 13. doi:10.1371/journal.ppat.1006700.

Stanaway, J.D., A. Parisi, K. Sarkar, B.F. Blacker, R.C. Reiner, S.I. Hay, M.R. Nixon, C. Dolecek, S.L. James, A.H. Mokdad, G. Abebe, E. Ahmadian, F. Alahdab, B.T.T. Alemnew, V. Alipour, F. Allah Bakeshei, M.D. Animut, F.

Ansari, J. Arabloo, E.T. Asfaw, M. Bagherzadeh, Q. Bassat, Y.M.M. Belayneh, F. Carvalho, A. Daryani, F.M. Demeke, A.B.B. Demis, M. Dubey, E.E. Duken, S.J. Dunachie, A. Eftekhari, E. Fernandes, R. Fouladi Fard, G.A. Gedefaw, B. Geta, K.B. Gibney, A. Hasanzadeh, C.L. Hoang, A. Kasaeian, A. Khater, Z.T. Kidanemariam, A.M. Lakew, R. Malekzadeh, A. Melese, D.T. Mengistu, T. Mestrovic, B. Miazgowski, K.A. Mohammad, M. Mohammadian, A. Mohammadian-Hafshejani, C.T. Nguyen, L.H. Nguyen, S.H. Nguyen, Y.L. Nirayo, A.T. Olagunju, T.O. Olagunju, H. Pourjafar, M. Qorbani, M. Rabiee, N. Rabiee, A. Rafay, A. Rezapour, A.M. Samy, S.G. Sepanlou, M.A. Shaikh, M. Sharif, M. Shigematsu, B. Tessema, B.X. Tran, I. Ullah, E.M. Yimer, Z. Zaidi, C.J.L. Murray, and J.A. Crump. 2019. The global burden of non-typhoidal salmonella invasive disease: a systematic analysis for the Global Burden of Disease Study 2017. *The Lancet Infectious Diseases*. 19:1312–1324. doi:10.1016/S1473-3099(19)30418-9.

Sturm, A., M. Heinemann, M. Arnoldini, A. Benecke, M. Ackermann, M. Benz, J. Dormann, and W.D. Hardt. 2011. The cost of virulence: Retarded growth of salmonella typhimurium cells expressing type iii secretion system 1. *PLoS Pathogens*. 7. doi:10.1371/journal.ppat.1002143.

Toller, I.M., M. Altmeyer, E. Kohler, M.O. Hottiger, and A. Müller. 2010. Inhibition of ADP ribosylation prevents and cures Helicobacter-induced gastric preneoplasia. *Cancer Research*. 70:5912–5922. doi:10.1158/0008-5472.CAN-10-0528.

Vida, A., G. Kardos, T. Kovács, B.L. Bodrogi, and P. Bai. 2018. Deletion of poly(ADP-ribose) polymerase-1 changes the composition of the microbiome in the gut. *Molecular Medicine Reports*. 18:4335–4341. doi:10.3892/mmr.2018.9474.

Wang, M., I.H. Qazi, L. Wang, G. Zhou, and H. Han. 2020. Salmonella virulence and immune escape. *Microorganisms*. 8:1–25. doi:10.3390/microorganisms8030407.

Xu, F., Y. Sun, S.Z. Yang, T. Zhou, N. Jhala, J. McDonald, and Y. Chen. 2019. Cytoplasmic PARP-1 promotes pancreatic cancer tumorigenesis and resistance. *International Journal of Cancer*. 145:474–483. doi:10.1002/ijc.32108.

Yunna, C., H. Mengru, W. Lei, and C. Weidong. 2020. Macrophage M1/M2 polarization. *European Journal of Pharmacology*. 877. doi:10.1016/j.ejphar.2020.173090.